NTNU

Transport of ferromagnetic domain walls

Vetle Meland Risinggård

Nanotechnology
Submission date: December 19, 2014
Supervisor: Jacob Linder, IFY

Norwegian University of Science and Technology
Department of Physics

Abstract

Inspired by recent work in the transport theory of ferromagnetic domain walls in nanowires we examine domain wall motion driven by external fields, currents and magnons using an analytic approach to the Landau-Lifshitz-Gilbert equation. Our discussion of field and current induced motion includes a comprehensive approach to domain wall extension and contraction, and our discussion of magnon induced motion includes a treatment of Gilbert damping. Numerical integration of the collective coordinate equations agrees with the analytical results. The mechanism and conditions for Walker breakdown in magnon induced domain wall motion as well as the effect of Dzyaloshinskii-Moriya and spin-orbit interactions on magnon induced motion are suggested as topics for further studies.

Contents

1 Introduction

Transport of ferromagnetic domain walls is just one area of the much larger field of magnetization dynamics. Magnetization dynamics is a rich and interesting topic from a fundamental physics point of view. It is rich in the same sense as fluid dynamics; a single system governed by one set of equations admits all manners of behavior from laminar flow to turbulence to various wave phenomena. There is much to explore. Similarly, there is a plethora of dynamical structures admitted in magnetization dynamics, such as spin-waves, elliptic function waves, solitons, dromions, vortices, spatio-temporal patterns and chaos [1]. The multitude of phenomena is also what makes magnetization dynamics so interesting. It means the field is far from being exhausted of new topics and is a complex and challenging field.

Lately, the interest in magnetization dynamics has increased due to novel applications in computer technology [2]. Magnetic patterns offer the possibility of non-volatile memories and are important in existing technologies such as hard disk drives and magnetic random access memories (MRAM). These technologies rely on field induced magnetization dynamics. Recent interest is rather focused on current induced magnetization dynamics [3–5]. A major advantage of controlling magnetization dynamics using currents instead of fields is that the resulting technology scales better [3]. As the bit size is reduced, its coercive field must be increased to retain stability with regard to thermal fluctuations. If the bit is controlled using Ørsted fields, the current must increase with the coercive field, while at the same time the wire cross-section decreases. In contrast, if the bit is controlled using spin-transfer torques the necessary current is expected to scale in proportion to the energy barrier for magnetization reversal—not to the bit dimension. As the bit size decreases to accommodate higher memory densities technologies based on current induced dynamics become more competitive. Commercial STT-MRAMs have already been introduced [6].

Another advantage related to controlling the magnetization dynamics using currents instead of fields is that it allows for precise spatial control of the applied magnetic torque. The racetrack memory is a novel magnetic memory that relies

on the manipulation of domain walls in nanowires using nanosecond current pulses [7]. Because tens of domain walls can be stored in each wire, a vertical integration of nanowire arrays is expected to offer dense mass storage. As with MRAMs, magnetic tunnel junctions (MTJs) can be used for reading. Successful operation of such magnetic shift registers has been reported [8].

In general, memories based on MJTs can be integrated with logic CMOS circuits in the interconnection layer because they consist entirely of metals and insulators. This opens the possibility for entirely new IC architectures, possibly reducing power consumption and interconnection delays [3, 9]. It has also been suggested that magnetic domain walls can be used to produce logic circuits [10].

To pursue technologies based on ferromagnetic domain wall motion it is necessary to move domain walls at high velocities in a controlled fashion. This requires an understanding of the microscopic mechanisms involved [11–15] as well as finding practical solutions to achieve the necessary speed [16]. Current induced domain wall motion requires high current densities, leading to problems with Joule heating [17]. While the domain wall velocity increases with current density, too high current densities can also deform the wall and degrade the information it carries. This phenomenon is named Walker breakdown and limits the useful domain wall velocities that are available [13, 18].

In order to solve such problems we seek novel mechanisms for domain wall motion, such as domain walls propagated by spin-waves (so-called all-magnonic domain wall propagation) [19]. In particular, spin-wave excitations of the magnetic lattice is possible in ferromagnetic insulators. While this removes issues related to Joule heating, it requires a mechanism that couples the magnetic components to electronic components, such as logic circuits.

This work is concerned with ferromagnetic domain wall transport in nanowires. We take an analytical approach, using the Landau-Lifshitz-Gilbert equation to describe the dynamic state of the magnetization. By limiting our scope to a one-dimensional assessment of transport phenomena we obtain tractable analytical equations, but we are also motivated by recent trends in experimental and numerical studies. While early works often involved domain walls in extended films, recent works have turned to nanowires because they offer greater control of domain walls, they are ideally suited to carry currents, and their dimensions are amenable to numerical studies [20].

2 The micromagnetic model

The micromagnetic model is a semi-classical continuum model that is used to describe the magnetization dynamics of ferromagnetic materials such as the transition metal ferromagnets Co, Fe and Ni and their alloys, such as permalloy [21]. This model is used to describe the magnetization dynamics at mesoscopic length scales [22, 23], that is, between tens of nanometers and micrometric length scales. The upper limit is only determined by convenience and the necessary level of detail in the description. On the other hand, the lower limit is due to the fundamental assumptions of the model; the model represents a continuum description and matter is ultimately made up from atoms. Thus the micromagnetic model provides a bridge between the quantum mechanical description and classical electrodynamics[1]. The classical mean-field treatment used in the model precludes the description of quantum mechanical fluctuations and magnetic inhomogeneity at the atomic scale.

The time-dynamics of the micromagnetic model is governed by the Landau-Lifshitz-Gilbert (LLG) equation. In this chapter we introduce the LLG equation, review the different terms that contribute to the effective magnetic field and show an example of a domain wall structure that might result from solving the LLG equation with the appropriate boundary conditions.

2.1 The Landau-Lifshitz-Gilbert equation

The equation that is now known as the Landau-Lifshitz-Gilbert equation first appeared as a modified form of the Landau-Lifshitz equation [25] in a paper prepared for the first Conference on Magnetism and Magnetic Materials in 1955 by Kelly and Gilbert [26]. A brief account due to Gilbert was published the same year [27]. This work was part of the graduate work of Gilbert, who in 1956 submitted his PhD thesis to Illinois Institute of Technology. In his thesis—which was never

[1] Herring and Kittel [24] discuss the relation between the atomic view and the continuum theory in some detail.

published—he gave the full account of a new equation of motion of the magnetization field in a ferromagnet. His motivation to derive such an equation was to resolve the problem of using the Landau-Lifshitz damping term for large damping. Our presentation of the LLG equation will follow the approach of reference [28], which is a condensed version of the key results from Gilbert's thesis that appeared in IEEE's *Classics in Magnetics* series.

2.1.1 Field equations for an undamped magnetization field

Our first step is to construct the equation of motion for the undamped magnetization field. We consider first a single magnetic moment

$$\widehat{\boldsymbol{m}} = \gamma \widehat{\boldsymbol{S}}, \tag{2.1}$$

where γ is the gyromagnetic ratio ($\gamma < 0$ for an electron spin) and $\widehat{\boldsymbol{m}}$ and $\widehat{\boldsymbol{S}}$ are the quantum mechanical magnetic moment and spin operators, respectively. By taking the expectation values of the operators (using appropriate quantum states or a density matrix) we can make a classical theory for the spin system. The equation of motion of a quantum mechanical expectation value is [29]

$$\partial_t \langle F \rangle = \frac{i}{\hbar} \left\langle [\widehat{H}, \widehat{F}] \right\rangle. \tag{2.2}$$

We take the Hamiltonian to be the general Hamiltonian for the interaction of a spin and a magnetic field,

$$\widehat{H} = -\gamma \boldsymbol{H} \cdot \widehat{\boldsymbol{S}}, \tag{2.3}$$

where $\boldsymbol{H}$ is the magnetic field. If we assume that the spin operator fulfill the standard algebra [30]

$$[\widehat{S}_a, \widehat{S}_b] = i\hbar \epsilon_{abc} \widehat{S}_c, \tag{2.4}$$

where ϵ_{abc} is the totally antisymmetric tensor (Levi-Civita symbol) [31], we get a cross product when we evaluate the commutator:

$$[\widehat{H}, \widehat{\boldsymbol{S}}]_b = -\gamma [H_a \widehat{S}_a, \widehat{S}_b] = -\gamma H_a [\widehat{S}_a, \widehat{S}_b] = -i\hbar\gamma \epsilon_{abc} H_a \widehat{S}_c = -i\hbar\gamma (\widehat{\boldsymbol{S}} \times \boldsymbol{H})_b.$$

If this cross product is substituted back into the equation of motion (2.2) we get

$$\partial_t \langle \boldsymbol{S} \rangle = \gamma \langle \boldsymbol{S} \rangle \times \boldsymbol{H}.$$

This equation can also be written in terms of the magnetic moment. In the following we drop the brackets $\langle \cdots \rangle$ and write

$$\partial_t \boldsymbol{m} = \gamma \boldsymbol{m} \times \boldsymbol{H}. \tag{2.5}$$

Our conclusion is that the magnetic moment will precess about the applied magnetic field [32, 33]. Its motion is illustrated in Figure 2.1a.

This result we could have expected—it is simply the classical equation $\partial_t \boldsymbol{L} = \boldsymbol{\tau}$ for a magnetic moment in an external magnetic field, and Ehrenfest's theorem from quantum mechanics guarantees that the equations of motion for quantum mechanical expectation values coincides with the classical equations of motion [29].

A key observation is that (2.5) is not only limited to the torque exerted by an external magnetic field. Any torque on the magnetic moment that is the result of a conservative force can be written in this form if we define the effective magnetic field

$$\boldsymbol{H} = -\left[\frac{\partial U(\boldsymbol{m})}{\partial m_x}\boldsymbol{e}_x + \frac{\partial U(\boldsymbol{m})}{\partial m_y}\boldsymbol{e}_y + \frac{\partial U(\boldsymbol{m})}{\partial m_z}\boldsymbol{e}_z\right] = -\frac{\partial U(\boldsymbol{m})}{\partial \boldsymbol{m}}, \tag{2.6}$$

where $U(\boldsymbol{m})$ is the potential from which the force is derived. The functional forms of different torque-exerting fields are explored in section 2.2.

We consider next a discrete set of magnetic moments, $\boldsymbol{m}_i$, $i = 1, 2, \ldots, n$, for which the equations of motion become

$$\partial_t \boldsymbol{m}_i = \gamma \boldsymbol{m}_i \times \boldsymbol{H}_i, \tag{2.7}$$

where the effective field on each magnetic moment is dependent on all the other magnetic moments,

$$\boldsymbol{H}_i = -\partial U(\boldsymbol{m}_1, \boldsymbol{m}_2, \ldots, \boldsymbol{m}_n)/\partial \boldsymbol{m}_i. \tag{2.8}$$

Note that the convention set down in equation (2.1) is such that the gyromagnetic ratio is negative for electron dominated systems, $\gamma < 0$. The opposite convention is to let the gyromagnetic ratio be positive and explicitly write out the minus sign—which is indeed the most common convention in the literature.

Finally we consider a continuous magnetization field $\boldsymbol{m}(\boldsymbol{r}, t)$. We define this field such that $\boldsymbol{m}(\boldsymbol{r}_i) = \boldsymbol{m}_i/\Delta r_i$ where the magnetic moments $\boldsymbol{m}_i$ are located at lattice points $\boldsymbol{r}_i$ and the lattice cell volume is Δr_i. This definition assumes that the magnetization field is smooth on the atomic scale[2]. If we substitute $\boldsymbol{m}_i = \boldsymbol{m}(\boldsymbol{r}_i)\Delta r_i$ into equations (2.7) and (2.8) and let $\Delta r_i \to 0$ sums become integrals, functions $U(\boldsymbol{m}_1, \boldsymbol{m}_2, \ldots, \boldsymbol{m}_n)$ become functionals $U[\boldsymbol{m}(\boldsymbol{r})]$ and derivatives $\partial U(\boldsymbol{m}_1, \boldsymbol{m}_2, \ldots, \boldsymbol{m}_n)/\partial \boldsymbol{m}_i$ become functional derivatives $\delta U[\boldsymbol{m}(\boldsymbol{r})]/\delta \boldsymbol{m}(\boldsymbol{r})$. This leads to the equation of motion of the magnetization field

$$\partial_t \boldsymbol{m}(\boldsymbol{r}, t) = \gamma \boldsymbol{m}(\boldsymbol{r}, t) \times \boldsymbol{H}(\boldsymbol{r}, t), \tag{2.9}$$

[2]We realize that this model cannot be applied to electrons in the conduction bands, for which the localization of the orbital is not well-defined. However, in transition metal ferromagnets the unpaired electron spins are all found in energy bands corresponding to the d and f orbitals for which localized orbitals is a good approximation. Contributions from the conduction electrons are taken into account using the *sd*-model which is treated in section 3.1.

The contribution from orbital angular momentum to the magnetic moment can be taken into account by adjusting the gyromagnetic ratio. Ralph and Stiles [4] quote typical g-factors to be between 2.1 and 2.2 with $\gamma < 0$. Similar numbers are found in Kittel [34].

where

$$\boldsymbol{H}(\boldsymbol{r},t) = -\frac{\delta U[\boldsymbol{m}(\boldsymbol{r},t)]}{\delta \boldsymbol{m}(\boldsymbol{r},t)}. \tag{2.10}$$

These equations are classical field equations that determine the motion of the magnetization field.

An important property of the effective field is that contributions stemming from different physical mechanisms add, so the total effective field felt by the magnetic moment is simply the vector sum. This is a result of the fact that the potentials add and that differentiation is a linear operation. Gilbert quotes five contributions to the so-called Stoner-Wohlfarth energy, namely the external field energy U_0, the demagnetization energy U_d, the exchange energy U_ex, the anisotropy energy U_a and the magnetoelastic energy U_me,

$$U = U_0 + U_\mathrm{d} + U_\mathrm{ex} + U_\mathrm{a} + U_\mathrm{me}.$$

The details of all these contributions will be treated in section 2.2.

2.1.2 Field equations for a damped magnetization field

The rate of remagnetization of a ferromagnet is limited by damping mechanisms involving a loss of energy from the macroscopic motion of the local magnetization field to microscopic thermal motion. A range of mechanisms might be involved, but eventually the energy is lost to phonons, magnons and thermal excitation of conduction electrons. We circumvent the problem of identifying the exact mechanism of the energy loss by constructing a phenomenological damping term. The phenomenological damping parameter we introduce will correspond to the rate of energy transfer and can be determined experimentally without knowing the details of the transfer mechanism.

We can introduce a dissipative term by formulating the problem in terms of a Lagrangian. Lagrange's equation of motion for a conservative system is

$$\frac{\mathrm{d}}{\mathrm{d}t}\frac{\delta L[\boldsymbol{m},\dot{\boldsymbol{m}}]}{\delta \dot{\boldsymbol{m}}} - \frac{\delta L[\boldsymbol{m},\dot{\boldsymbol{m}}]}{\delta \boldsymbol{m}} = 0, \tag{2.11}$$

where the dot denotes a time derivative. By introducing the Rayleigh dissipation functional

$$R = \frac{\eta}{2}\int \dot{\boldsymbol{m}}\cdot\dot{\boldsymbol{m}}\mathrm{d}\boldsymbol{r} \tag{2.12}$$

we get Lagrange's equation of motion for a dissipative system [32],

$$\frac{\mathrm{d}}{\mathrm{d}t}\frac{\delta L[\boldsymbol{m},\dot{\boldsymbol{m}}]}{\delta \dot{\boldsymbol{m}}} - \frac{\delta L[\boldsymbol{m},\dot{\boldsymbol{m}}]}{\delta \boldsymbol{m}} + \frac{\delta R[\dot{\boldsymbol{m}}]}{\delta \dot{\boldsymbol{m}}} = 0. \tag{2.13}$$

The parameter η quantifies the average damping throughout the sample. When we take η to be a scalar we assume that the damping is uniform in the sample. The rate of energy loss due to the dissipative force is [32]

$$\frac{\mathrm{d}W}{\mathrm{d}t} = 2R[\dot{\boldsymbol{m}}] = \eta \int \dot{\boldsymbol{m}} \cdot \dot{\boldsymbol{m}} \mathrm{d}\boldsymbol{r}. \tag{2.14}$$

The Lagrangian for the system is $L[\boldsymbol{m}, \dot{\boldsymbol{m}}] = T[\boldsymbol{m}, \dot{\boldsymbol{m}}] - U[\boldsymbol{m}]$. If we insert this into (2.13) and use $\delta U[\boldsymbol{m}]/\delta \dot{\boldsymbol{m}} = 0$ and $\delta R[\dot{\boldsymbol{m}}]/\delta \dot{\boldsymbol{m}} = \eta \dot{\boldsymbol{m}}$ we obtain the equation

$$\frac{\mathrm{d}}{\mathrm{d}t} \frac{\delta T[\boldsymbol{m}, \dot{\boldsymbol{m}}]}{\delta \dot{\boldsymbol{m}}} - \frac{\delta T[\boldsymbol{m}, \dot{\boldsymbol{m}}]}{\delta \boldsymbol{m}} + [-\boldsymbol{H} + \eta \boldsymbol{m}] = 0. \tag{2.15}$$

If there was no damping we would have $\eta = 0$ and (2.15) should be equivalent to (2.9). We note that the effect of adding a damping term in the Lagrangian formulation is to reduce the effective magnetic field and change the torque exerted on the magnetization field. Thus it is reasonable that for $\eta \neq 0$ we get an equation of motion for the damped magnetization field that is analogous to equation (2.9), but with a magnetic field that is reduced by the damping field $-\eta \dot{\boldsymbol{m}}$,

$$\partial_t \boldsymbol{m}(\boldsymbol{r}, t) = \gamma \boldsymbol{m}(\boldsymbol{r}, t) \times [\boldsymbol{H}(\boldsymbol{r}, t) - \eta \partial_t \boldsymbol{m}(\boldsymbol{r}, t)]. \tag{2.16}$$

This is the Landau-Lifshitz-Gilbert equation. The effect of the damping field is illustrated in Figure 2.1b.

An important feature of the LLG equation is that it can only be used to study changes in the magnetization direction and not changes in the length of the magnetization vector. This can be seen by multiplying the equation with $\boldsymbol{m}$,

$$\tfrac{1}{2} \partial_t \boldsymbol{m}^2 = \boldsymbol{m} \cdot \partial_t \boldsymbol{m} = \boldsymbol{m} \cdot \gamma \boldsymbol{m} \times [\boldsymbol{H} - \eta \partial_t \boldsymbol{m}] = 0,$$

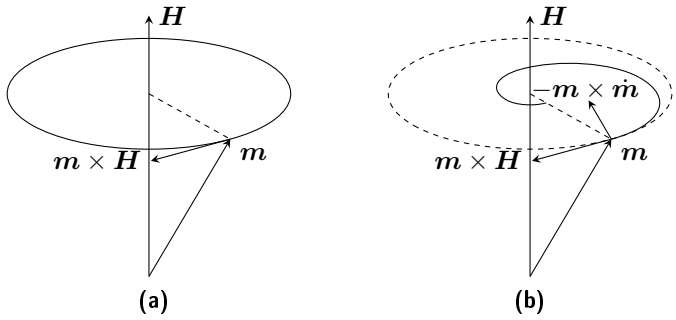

Figure 2.1: Precession of a magnetic moment $\boldsymbol{m}$ about a magnetic field $\boldsymbol{H}$. Undamped motion (a) and damped motion (b). Under the torque $\gamma \boldsymbol{m} \times \boldsymbol{H}$ the tip of the magnetization vector traces out a circle. When the damping field $-\eta \dot{\boldsymbol{m}}$ is added, the magnetization vector will instead spiral into alignment with the magnetic field.

since $\boldsymbol{m} \times \boldsymbol{H} \perp \boldsymbol{m}$ and $\boldsymbol{m} \times \partial_t \boldsymbol{m} \perp \boldsymbol{m}$. We conclude that the saturation magnetization $m = |\boldsymbol{m}(\boldsymbol{r}, t)|$ is a constant. It is common to write the damping parameter in terms of m, $\gamma\eta = \alpha/m$, giving

$$\partial_t \boldsymbol{m}(\boldsymbol{r}, t) = \gamma \boldsymbol{m}(\boldsymbol{r}, t) \times \boldsymbol{H}(\boldsymbol{r}, t) - \frac{\alpha}{m} \boldsymbol{m}(\boldsymbol{r}, t) \times \partial_t \boldsymbol{m}(\boldsymbol{r}, t). \tag{2.17}$$

Note that it follows from our convention (2.1) that the gyromagnetic ratio γ and Gilbert damping constant α are both negative in electron dominated systems.

2.2 Stoner-Wohlfarth energy and the effective field

The potential energy of the magnetization field is commonly referred to as the Stoner-Wohlfarth energy in recognition of the work of Stoner and Wohlfarth [35] in using the potential energy functional to elucidate the domain structure in ferromagnets. Gilbert identifies five contributions to the Stoner-Wohlfarth energy, namely the external field energy U_0, the demagnetization energy U_d, the exchange energy U_ex, the anisotropy energy U_a and the magnetoelastic energy U_me,

$$U = U_0 + U_\mathrm{d} + U_\mathrm{ex} + U_\mathrm{a} + U_\mathrm{me}. \tag{2.18}$$

The two former terms correspond to magnetic fields while the three latter correspond to effective fields that are quantum mechanical in origin.

2.2.1 External field energy

The energy related to the external field is also known as the Zeeman energy. The interaction of the magnetization with an external magnetic field was the starting point of our analysis back in subsection 2.1.1 that led to the LLG equation. An external field $\boldsymbol{H}_0$ has the energy functional

$$U_0[\boldsymbol{m}(\boldsymbol{r}, t)] = -\int \boldsymbol{m}(\boldsymbol{r}, t) \cdot \boldsymbol{H}_0 \mathrm{d}\boldsymbol{r} \tag{2.19}$$

because

$$-\frac{\delta U_0[\boldsymbol{m}(\boldsymbol{r}, t)]}{\delta \boldsymbol{m}(\boldsymbol{r}, t)} = \boldsymbol{H}_0.$$

2.2.2 Demagnetization energy

The demagnetization energy is due to the interaction of the magnetization field with itself. Think of the case of a bar magnet. As the magnetization of the bar increases the magnetic field that is emanating from the bar increases too. Since the divergence of the magnetic field must be zero the magnetic field lines will form closed loops going from the north pole to the south pole. But some of the field from the surface poles will pass through the interior of the material, opposing the magnetization that created it in the first place. This field is named the

demagnetization field. Magnetostatic effects are discussed in detail by O'Handley [36].

The demagnetization field $\boldsymbol{H}_\mathrm{d}$ can be written as

$$\boldsymbol{H}_\mathrm{d} = -N\boldsymbol{m}, \tag{2.20}$$

where N is the demagnetization tensor. If the body is ellipsoidal the demagnetization tensor is diagonal and the demagnetization field is

$$\boldsymbol{H}_\mathrm{d} = -N_x m_x \boldsymbol{e}_x - N_y m_y \boldsymbol{e}_y - N_z m_z \boldsymbol{e}_z.$$

Here, N_x, N_y, N_z are the diagonal elements of the demagnetization tensor. The demagnetization field is uniform and constant inside an ellipsoid, but is more complicated for other geometrical shapes. For a given demagnetization field $\boldsymbol{H}_\mathrm{d}$ we have the energy functional

$$U_\mathrm{d}[\boldsymbol{m}(\boldsymbol{r},t)] = -\frac{\mu_0}{2}\int \boldsymbol{m}(\boldsymbol{r},t)\cdot\boldsymbol{H}_\mathrm{d}\mathrm{d}\boldsymbol{r}. \tag{2.21}$$

Again, in the case of an ellipsoid the demagnetization energy is

$$U_\mathrm{d}[\boldsymbol{m}(\boldsymbol{r},t)] = \frac{\mu_0}{2}\int (N_x m_x^2 + N_y m_y^2 + N_z m_z^2)\mathrm{d}\boldsymbol{r},$$

where μ_0 is the magnetic permeability of vacuum. This energy functional has the same form as an uniaxial magnetocrystalline anisotropy energy (2.27), which we are going to look into in subsection 2.2.4, so if we are dealing with an ellipsoid we may absorb the contribution from the demagnetization energy into the contribution from the magnetic anisotropy; this is named a magnetic shape anisotropy. A nanowire with a high aspect ratio can be approximated as an infinitely long cylinder. Since an infinitely long cylinder is the limiting form of a prolate ellipsoid, demagnetization effects can in fact be treated as simple uniaxial shape anisotropies in the remainder of this text. For the sake of an example, let the wire axis be the x-axis of our coordinate system. Then $N_x \to 0$ as the aspect ratio of the wire goes to infinity and it is easy to magnetize it along the x-axis (no demagnetization energy) and harder to magnetize it in the yz-plane (where there actually is a contribution from the demagnetization energy). The implication of this is that we can take proper care of demagnetization effects simply by letting the x-axis be an easy axis in our calculations.

2.2.3 Exchange energy

Spin alignment in ferromagnets occurs because unpaired electron spins lower their Coulomb repulsion by having an anti-symmetric spatial wave function under particle exchange [29, 37]. Since the total electron wave function must be overall anti-symmetric the electron spins align, producing a macroscopically appreciable magnetic moment. So ferromagnetic coupling comes about as a result of a

minimization of the electrostatic interaction, not as a result of magnetic dipolar coupling. Since the ferromagnetic coupling favors spin alignment it is important to the dynamics of the magnetization vector. We are going to use a very simple model for the ferromagnetic exchange, namely the quantum Heisenberg model. For a discrete lattice of spins the Heisenberg Hamiltonian can be written ($J > 0$) [37]

$$\widehat{H} = -J \sum_{\langle i,j \rangle} \widehat{\boldsymbol{S}}_i \cdot \widehat{\boldsymbol{S}}_j, \tag{2.22}$$

where the sum runs over nearest neighbors on the lattice and J is known as the exchange integral. However, the LLG equation involves a continuous magnetization field so we must find the exchange energy in the continuous limit. Our approach follows the approach of Mulazzi *et al.* [38].

For simplicity we consider a one-dimensional model—a linear chain of classical spins spaced a apart,

$$H = -2J \sum_i \boldsymbol{S}_i \cdot \boldsymbol{S}_{i+1}. \tag{2.23}$$

Consider now the situation where all the spins are aligned and one of the spins is rotated with respect to the others with its magnitude conserved (as might be the result of the thermal excitation of a magnon). Then we may write

$$H \approx -2JS^2 \sum_i \cos(\vartheta_i - \vartheta_{i+1}).$$

If we only consider long wavelength excitations—so that the angles between the neighboring spins are small—we can write $\vartheta_i - \vartheta_{i+1} = \delta\vartheta_i$ and expand the cosine using a Taylor series that is truncated at second order,

$$\cos \delta\vartheta_i \approx 1 - \frac{\delta\vartheta_i^2}{2} + \dots$$

The sum is then

$$H \approx -2JS^2 \sum_i \left(1 - \frac{\delta\vartheta_i^2}{2}\right) = E_0 + \Delta H.$$

The first term is simply the constant energy of having all the spins aligned. The second term,

$$\Delta H = JS^2 \sum_i \delta\vartheta_i^2,$$

is the energy necessary for creating the deviation from the ground-state. The small variable $\delta\vartheta_i$ can be regarded as the spin magnitude perpendicular to the main component S. If we go to the continuum limit so that the lattice of spins $\boldsymbol{S}_i$

at long wavelength excitations can be approximated by a magnetization field $\boldsymbol{m}(r)$ then $\delta\vartheta_i$ must be identified with the derivative $(a/m)\mathrm{d}\boldsymbol{m}(r)/\mathrm{d}r$. In the continuum limit, then,

$$\Delta H = \frac{JS^2a^2}{m^2}\int\left[\frac{\mathrm{d}\boldsymbol{m}(r)}{\mathrm{d}r}\right]^2\mathrm{d}r. \tag{2.24}$$

The generalization to three dimensions simply changes the prefactor (coordination number) and the total derivative changes into a gradient,

$$U_{\mathrm{ex}}[\boldsymbol{m}(\boldsymbol{r},t)] = \frac{A}{m^2}\int\left[(\nabla m_x)^2+(\nabla m_y)^2+(\nabla m_z)^2\right]\mathrm{d}\boldsymbol{r}, \tag{2.25}$$

where A is known as the exchange stiffness, $A>0$. The effective field due to the exchange interaction is then

$$\boldsymbol{H}_{\mathrm{ex}}[\boldsymbol{m}(\boldsymbol{r},t)] = -\frac{\delta U_{\mathrm{ex}}[\boldsymbol{m}(\boldsymbol{r},t)]}{\delta\boldsymbol{m}(\boldsymbol{r},t)} = \frac{2A}{m^2}\nabla^2\boldsymbol{m}(\boldsymbol{r},t). \tag{2.26}$$

It is easy to see that in the discrete case the Heisenberg Hamiltonian (2.22) promotes spin alignment. In the continuous case (2.25) we observe that a non-uniform magnetization (non-zero gradient) involves an energy penalty.

2.2.4 Magnetic anisotropy energy

When a physical property of a material is a function of direction, that property is said to exhibit anisotropy. When there is a preference for magnetization in a certain direction, we speak of magnetic anisotropy. The sources of magnetic anisotropy are diverse. Magnetostatic effects such as the demagnetization field from subsection 2.2.2 gives rise to shape anisotropies. Another source of magnetic anisotropy is magnetocrystalline anisotropy, for which the magnetization is preferentially directed along specific crystallographic axes.

Magnetocrystalline anisotropy is discussed in detail by for example O'Handley [36]. Without any regard for the physical mechanism behind magnetocrystalline anisotropy it is clear that the magnetocrystalline anisotropy energy can be visualized as a three-dimensional surface in spherical coordinates: the angular coordinates (ϑ,φ) gives the orientation of the magnetization vector and the radial coordinate r gives the value of the anisotropy energy. This surface can be approximated by expansions in sines and cosines of the angles. In particular, it can be written as an expansion in the Legendre polynomials of the direction cosines of the magnetization vector since the Legendre polynomials are complete (total) and orthonormal on the interval $[-1,+1]$ [39]. To first order, a uniaxial magnetocrystalline anisotropy can be written as

$$U_{\mathrm{a}}[\boldsymbol{m}(\boldsymbol{r},t)] = \frac{k}{m^2}\int m_i^2\mathrm{d}\boldsymbol{r}. \tag{2.27}$$

$k < 0$ implies an easy axis and $k > 0$ implies an easy plane (hard axis). Cubic anisotropies are more difficult to deal with, since they involve three direction cosines and we must invoke the point group symmetry of the crystal to reduce the number of independent terms. To first order the magnetocrystalline energy density of a cubic system may be written as

$$u_{\mathrm{a}}[\boldsymbol{m}(\boldsymbol{r},t)] = (k/m^4)(m_x^2 m_y^2 + m_y^2 m_z^2 + m_z^2 m_x^2). \tag{2.28}$$

In order to understand the physical mechanism behind magnetocrystalline anisotropy we must understand how the magnetic moments of the lattice can distinguish between the different crystallographic directions. Such an effect requires a coupling between spin space and real space; spin-orbit interaction. It is necessary for the spin-orbit interaction to produce magnetocrystalline anisotropy that there is also a coupling between the orbital angular momentum and the crystal field (electric field distribution in the crystal). Such a coupling is provided if the atoms have non-spherical charge distributions, *i.e.* if the z-component of the orbital angular momentum summed over all electrons in the atom is non-zero, $\langle L_z \rangle \neq 0$. Simply put, we have magnetocrystalline anisotropy if the orientation of the atom is locked to the lattice and the orientation of the spin is locked to the atom. Thus it is important for magnetocrystalline anisotropy that there is a significant directional character to the bonding. In some materials there can also be a contribution to magnetocrystalline anisotropy from magnetic dipolar interactions.

It is clear that the magnetocrystalline anisotropy is dependent on the local atomic environment. Without any further considerations of the mechanism behind magnetocrystalline anisotropy we can make a simple model of the magnetic anisotropy between two atoms by considering the angle between the magnetization and the vector from one of the atoms to the other. The anisotropy energy can be expanded as a series of Legendre polynomials in the cosine of this angle, and the coefficients of this series will be dependent on the distance between the atoms. In this way we can relate the macroscopic coefficient k in (2.27) to microscopic quantities; such a model is known as a pair interaction model. Again, the uniaxial anisotropy is given by (2.27) to first order.

In the remainder of this text we are going to consider a biaxial magnetic anisotropy energy given by

$$U_{\mathrm{a}}[\boldsymbol{m}(\boldsymbol{r},t)] = -\frac{1}{m^2}\int \left(K m_x^2 - K_\perp m_z^2\right) \mathrm{d}\boldsymbol{r}, \tag{2.29}$$

$K, K_\perp > 0$. The first term is an easy axis anisotropy contributed by for example the nanowire demagnetization energy. The second term is a hard axis anisotropy that can result from for instance magnetocrystalline or magnetoelastic anisotropy. The corresponding effective magnetic field is

$$\boldsymbol{H}_{\mathrm{a}}[\boldsymbol{m}(\boldsymbol{r},t)] = -\frac{\delta U_{\mathrm{a}}[\boldsymbol{m}(\boldsymbol{r},t)]}{\delta \boldsymbol{m}(\boldsymbol{r},t)} = \frac{2K}{m^2} m_x \boldsymbol{e}_x - \frac{2K_\perp}{m^2} m_z \boldsymbol{e}_z. \tag{2.30}$$

2.2.5 Magnetoelastic energy

We mentioned in subsection 2.2.4 that there is a relation between the crystallographic directions and the magnetization; this is the magnetocrystalline anisotropy. Now, the magnetocrystalline anisotropy is dependent on the crystal field. The crystal field will be changed if the crystal is strained by an external mechanical stress—such a strain will reduce its symmetry and also change its value. Therefore, mechanical stresses will affect the preferred magnetization direction in the presence of magnetocrystalline anisotropy. This effect is named the Villari effect. There is also the reciprocal effect; the magnetization process can cause the material to change its dimensions. This effect is named magnetostriction and was first observed by James Joule. Together, these effects show that there is a magnetoelastic coupling, and this coupling will contribute to the magnetic anisotropy. Magnetoelastic anisotropy is detailed by O'Handley [36] and by Kittel [40].

We follow Kittel's treatment of the magnetoelastic energy. The elastic energy density in a cubic crystal is given by

$$\begin{aligned} u_{\mathrm{el}} =& \tfrac{1}{2}c_{11}(e_{xx}^2 + e_{yy}^2 + e_{zz}^2) + \tfrac{1}{2}c_{44}(e_{xy}^2 + e_{yz}^2 + e_{zx}^2) \\ &+ c_{12}(e_{yy}e_{zz} + e_{xx}e_{zz} + e_{xx}e_{yy}), \end{aligned} \tag{2.31}$$

where c_{ij} are the elastic moduli and e_{ij} are strains. The magnetocrystalline anisotropy energy density for a cubic system (2.28) can be expanded as a Taylor series in the strains,

$$u_{\mathrm{a}} = (u_{\mathrm{a}})_0 + \sum_{i \geq j} \left(\frac{\partial u_{\mathrm{a}}}{\partial e_{ij}} \right)_0 e_{ij} + \ldots, \tag{2.32}$$

where the constant term must satisfy cubic symmetry, but the first order terms can have lower symmetry because they refer to the deformed lattice. If this is done and we only use the first order terms we get from symmetry considerations that

$$\begin{aligned} m^2 \partial u_{\mathrm{a}}/\partial e_{xx} &= B_1 m_x^2 & m^2 \partial u_{\mathrm{a}}/\partial e_{yy} &= B_1 m_y^2 \\ m^2 \partial u_{\mathrm{a}}/\partial e_{zz} &= B_1 m_z^2 & m^2 \partial u_{\mathrm{a}}/\partial e_{xy} &= B_2 m_x m_y \\ m^2 \partial u_{\mathrm{a}}/\partial e_{yz} &= B_2 m_y m_z & m^2 \partial u_{\mathrm{a}}/\partial e_{zx} &= B_2 m_z m_x \end{aligned} \tag{2.33}$$

where B_1 and B_2 are named the magnetoelastic coupling constants. The total energy density which depends on the strain and the crystallographic directions of the magnetization vector (elastic energy, magnetoelastic energy and magnetocrystalline energy) is then

$$\begin{aligned} u[\boldsymbol{m}(\boldsymbol{r},t)] =& (k/m^4)(m_x^2 m_y^2 + m_y^2 m_z^2 + m_z^2 + m_x^2) \\ &+ (B_1/m^2)(m_x^2 e_{xx} + m_y^2 e_{yy} + m_z^2 e_{zz}) \\ &+ (B_2/m^2)(m_x m_y e_{xy} + m_y m_z e_{yz} + m_z m_x e_{zx}) \\ &+ \tfrac{1}{2}c_{11}(e_{xx}^2 + e_{yy}^2 + e_{zz}^2) + \tfrac{1}{2}c_{44}(e_{xy}^2 + e_{yz}^2 + e_{zx}^2) \\ &+ c_{12}(e_{yy}e_{zz} + e_{xx}e_{zz} + e_{xx}e_{yy}). \end{aligned} \tag{2.34}$$

By minimizing this energy density functional with respect to the crystal strains for a given local magnetization it can be shown that the energy functional of the magnetoelastic anisotropy energy has a form that is similar to the uniaxial magnetocrystalline anisotropy energy density,

$$u = \frac{k+p}{m^4}(m_x^2 m_y^2 + m_y^2 m_z^2 + m_z^2 m_x^2), \tag{2.35}$$

where p is independent of the magnetization vector but is simply related to the elastic moduli and the magnetoelastic coupling constants. For the iron and nickel O'Handley quotes values of p/k to be about 0.1 % and 1 % respectively. This ratio is larger in the rare-earth alloys, *e.g.* it is 20 % in $TbFe_2$.

We conclude that contributions from the magnetoelastic anisotropy can be dropped altogether to a first approximation. Alternatively they can be treated in the same way as contributions from the demagnetization energy—we absorb them into a single magnetic anisotropy term that has the functional form of a magnetocrystalline anisotropy.

2.3 A static domain wall

We are now going to demonstrate that one of the static solutions to the LLG equation is a domain wall structure. We start out with the LLG equation

$$\partial_t \boldsymbol{m} = \gamma \boldsymbol{m} \times [\boldsymbol{H} - \eta \partial_t \boldsymbol{m}].$$

Since we are seeking a static solution to this equation we set $\partial_t \boldsymbol{m} = 0$ giving the simplified equation

$$\boldsymbol{m} \times \boldsymbol{H} = 0, \tag{2.36}$$

where $\boldsymbol{H}$ is understood to be the effective magnetic field in the solid. As $|\boldsymbol{m}| = m$ is a constant in time the magnetization vector must be rotating on a sphere and we can without loss of generality write

$$\boldsymbol{m} = m(\cos\vartheta \boldsymbol{e}_x + \cos\varphi \sin\vartheta \boldsymbol{e}_y + \sin\varphi \sin\vartheta \boldsymbol{e}_z), \tag{2.37}$$

see Figure 2.2.

We consider our nanowire to be a one-dimensional object whose axis lies along the x-axis. In the absence of an external field this allows us to consider only exchange interactions and magnetic anisotropy,

$$\boldsymbol{H} = \boldsymbol{H}_{\text{ex}} + \boldsymbol{H}_{\text{a}}, \tag{2.38}$$

where $\boldsymbol{H}_{\text{ex}}$ is given by (2.26) and $\boldsymbol{H}_{\text{a}}$ is given by (2.30). Note that the x-axis is the easy axis and the z-axis is the hard axis.

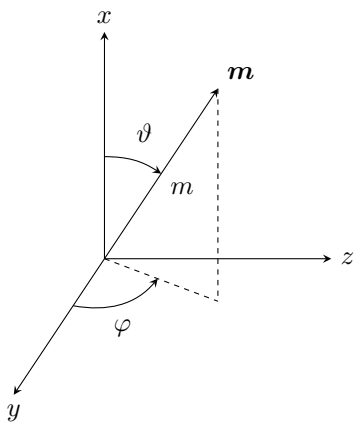

Figure 2.2: The magnetization vector in spherical coordinates.

The derivative we need to evaluate to calculate the exchange field can be found using

$$\nabla^2 \boldsymbol{m} = (\nabla \cdot \nabla)\boldsymbol{m} = (\partial_x^2 + \partial_y^2 + \partial_z^2)\boldsymbol{m} = \partial_x^2 \boldsymbol{m},$$

where we only let φ and ϑ change in the x-direction. First we do the x-component:

$$\partial_x^2 m_x/m = \partial_x^2 \cos\vartheta = \partial_x[-\sin\vartheta(\partial_x\vartheta)] = -\cos\vartheta(\partial_x\vartheta)^2 - \sin\vartheta(\partial_x^2\vartheta).$$

Then we do the y-component:

$$\begin{aligned}\partial_x^2 m_y/m =& \partial_x^2(\cos\varphi\sin\vartheta) = \partial_x[-\sin\varphi\sin\vartheta(\partial_x\varphi) + \cos\varphi\cos\vartheta(\partial_x\vartheta)] \\ =& -\cos\varphi\sin\vartheta(\partial_x\varphi)^2 - \sin\varphi\sin\vartheta(\partial_x^2\varphi) - 2\sin\varphi\cos\vartheta(\partial_x\varphi)(\partial_x\vartheta) \\ & -\cos\varphi\sin\vartheta(\partial_x\vartheta)^2 + \cos\varphi\cos\vartheta(\partial_x^2\vartheta).\end{aligned}$$

And finally we do the z-component:

$$\begin{aligned}\partial_x^2 m_z/m =& \partial_x^2(\sin\varphi\sin\vartheta) = \partial_x[\cos\varphi\sin\vartheta(\partial_x\varphi) + \sin\varphi\cos\vartheta(\partial_x\vartheta)] \\ =& -\sin\varphi\sin\vartheta(\partial_x\varphi)^2 + \cos\varphi\sin\vartheta(\partial_x^2\varphi) + 2\cos\varphi\cos\vartheta(\partial_x\varphi)(\partial_x\vartheta) \\ & -\sin\varphi\sin\vartheta(\partial_x\vartheta)^2 + \sin\varphi\cos\vartheta(\partial_x^2\vartheta).\end{aligned}$$

Before we try to evaluate the left-hand side of equation (2.36) we simplify the problem even more by considering only low energy solutions. The minimal energy solution to this problem is $\boldsymbol{m} = \pm m\boldsymbol{e}_x$. It is easy to see that this is a solution to the static LLG equation because then $\boldsymbol{H}_{\text{ex}} = 0$ and $\boldsymbol{H}_{\text{a}} = (2K/m)\boldsymbol{e}_x$ giving $\boldsymbol{H} = \boldsymbol{H}_{\text{ex}} + \boldsymbol{H}_{\text{a}} = (2K/m)\boldsymbol{e}_x$ and so $\boldsymbol{m} \times \boldsymbol{H} = 0$ since $\boldsymbol{m} \parallel \boldsymbol{H}$. Moreover, this solution minimizes both the exchange and anisotropy energies, making it the minimal energy solution. However, this solution is trivial there are other, more interesting low energy solutions. Since the z-axis is the hard axis solutions with $0 < \varphi < \pi$ or with $\pi < \varphi < 2\pi$ will have a higher energy that solutions for which

$\varphi = 0, \pi$. When studying low energy solutions we can thus require $\varphi = 0, \pi$, giving $\partial_x \varphi = 0$. Then, the magnetization vector reduces to

$$\boldsymbol{m} = m(\cos\vartheta \boldsymbol{e}_x \pm \sin\vartheta \boldsymbol{e}_y),$$

and the fields reduce to

$$\boldsymbol{H}_{\text{ex}} = -\frac{2A}{m}\left[\cos\vartheta(\partial_x\vartheta)^2 + \sin\vartheta(\partial_x^2\vartheta)\right]\boldsymbol{e}_x \pm \frac{2A}{m}\left[\cos\vartheta(\partial_x^2\vartheta) - \sin\vartheta(\partial_x\vartheta)^2\right]\boldsymbol{e}_y$$

and

$$\boldsymbol{H}_{\text{a}} = \frac{2K}{m}\cos\vartheta \boldsymbol{e}_x.$$

It is now time to evaluate the the left-hand side of equation (2.36). Since $m_z = 0$ and $H_z = 0$ necessarily $\boldsymbol{m} \times \boldsymbol{H} \parallel \boldsymbol{e}_z$. Carrying out the cross product, canceling terms and using $\cos^2\vartheta + \sin^2\vartheta = 1$ we find that our equation is then

$$A(\partial_x^2\vartheta) = K\cos\vartheta\sin\vartheta. \tag{2.39}$$

This equation could also have been obtained by considering the total magnetic energy as a volume integral of the energy density over the solid and minimizing this energy using the Euler equation as is done in the calculus of variations [25, 31]. Observing that $\partial_x \cos^2\vartheta = -2\cos\vartheta\sin\vartheta(\partial_x\vartheta)$ and $\partial_x(\partial_x\vartheta)^2 = 2(\partial_x\vartheta)(\partial_x^2\vartheta)$ we rewrite this equation as

$$\partial_x\left[A(\partial_x\vartheta)^2 + K\cos^2\vartheta\right] = 0$$

which can be integrated to give

$$\frac{A}{K}(\partial_x\vartheta)^2 + \cos^2\vartheta = c.$$

The constant of integration must be determined from the boundary conditions of the problem. We are considering low energy solutions and such solutions must have $\cos^2\vartheta \to 1$ as $x \to \pm\infty$ because of the easy axis anisotropy. In the limit $x \to \pm\infty$ we thus have $\partial_x\vartheta \to 0$ and the constant is determined to be $c = 1$. Taking the square root gives

$$\pm\lambda\partial_x\vartheta = \sqrt{1 - \cos^2\vartheta} = \sin\vartheta,$$

where we defined $\lambda = \sqrt{A/K}$. As $0 \le \vartheta \le \pi$ it follows that $\sin\vartheta \ge 0$ and the sign of $\partial_x\vartheta$ is unambiguous. This equation can easily be integrated using the tabulated integral

$$\int \frac{\mathrm{d}z}{\sin z} = \ln\tan\frac{z}{2} + c \tag{2.40}$$

and we find the solution

$$\vartheta(x) = 2\arctan\exp\left(\pm\frac{x-X}{\lambda}\right), \tag{2.41}$$

where X is the constant of integration. In the static solution we have found the angle ϑ goes from 0 at $x = \pm\infty$ to π at $x = \mp\infty$, see Figure 2.3. In other words: our static solution is a 180° domain wall at $x = X$. The choice of sign in the exponential determines the sign of $\partial_x\vartheta$; a positive sign gives $\partial_x\vartheta > 0$ and a negative sign gives $\partial_x\vartheta < 0$. The sign of $\partial_x\vartheta$ is commonly referred to as the topological charge of the domain wall, Q, because a wall with $Q = +1$ ($Q = -1$) will respond to an applied magnetic field pointing in the positive x-direction by moving in the positive (negative) x-direction. This is analogous to how a particle with positive (negative) electric charge moves parallel (anti-parallel) to an applied electric field. The relative strength of the Heisenberg coupling, A, to the anisotropy constant, K, namely $\lambda = \sqrt{A/K}$, is called the domain wall width. One more parameter characterizes the domain wall. Although the choice of having $\varphi = 0$ or $\varphi = \pi$ did not matter to the form of the solution $\vartheta(x)$ it does determine the direction in which the magnetization vector points at $x = X$, $\boldsymbol{m} = \pm m\boldsymbol{e}_y$. Thus, the choice of φ determines the handedness of the magnetization rotation in the domain wall and is named the chirality of the wall, $C = \pm 1$. If we choose right-handed rotation to define positive chirality it follows that $C = Q(1 - 2\varphi/\pi)$. A domain wall with positive topological charge and positive chirality is shown in Figure 3.2.

Domain walls are commonly classified as Bloch walls or Néel walls. In a one-dimensional domain wall structure, the magnetization only changes along one Cartesian axis; for instance this can be the x-axis, as was the case above. If the rotation of the magnetization vector takes place in a plane that is perpendicular to this axis—this would be the yz-plane in our example—we name the domain wall a Bloch wall. Alternatively, the axis along which the magnetization changes could lie in the plane of rotation of the magnetization vector. This was the case in our example: the magnetization changes along the x-axis and the magnetization vector rotates in the xy-plane. In that case, the domain wall is named a Néel wall.

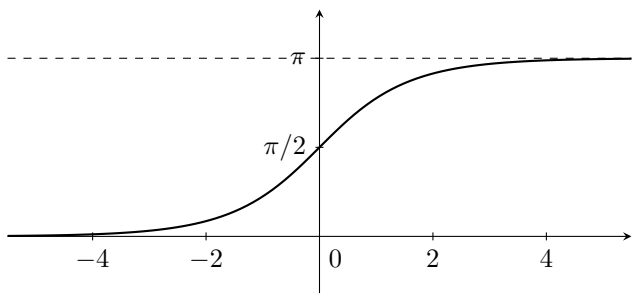

Figure 2.3: The solution $\vartheta(x) = 2\arctan\exp x$. Since $\partial_x\vartheta > 0$ the topological charge is $Q = +1$. The position of the domain wall is $X = 0$ and x is given in units of λ.

If we choose a positive topological charge the calculations above give a so-called head-to-head Néel wall; a negative topological charge gives a tail-to-tail Néel wall. We get Bloch walls when the easy plane is perpendicular to the axis along which the magnetization changes and Néel walls when the axis along which the magnetization changes lies in the easy plane. In the absence of interactions that correlates spin space and real space, like the spin-orbit interaction, the distinction between Bloch walls and Néel walls has no effect on phenomena like electron transport and spin torque [5, 41].

3 Domain wall motion under external fields and currents

Transport of ferromagnetic domain walls may be accomplished by letting the domain wall interact with an external magnetic field, a spin-polarized electric current or with magnons [19]. It is intuitively clear that a domain wall will move under an external magnetic field due to the gain in Zeeman energy. A detailed mechanism is described in section 3.3. However, domain wall motion due to currents or magnons requires more detailed investigations. We are going to treat domain wall motion due to currents in this chapter and save domain wall motion due to magnons for chapter 4.

Domain wall motion under currents is based on a mechanism known as spin-transfer torque [3, 4]. To understand this mechanism we must distinguish between the dynamics of the itinerant current-carrying electrons and the dynamics of the localized electrons that make up the local magnetization. The repolarization of a current that passes from one domain to the next causes the itinerant electrons to transfer spin angular momentum to the localized magnetic moments. The resulting torque rotates each of the localized moments by an angle and propagates the domain wall in the itinerant electron direction of travel.

In this chapter we are going to introduce the *sd*-model for separate dynamics of the itinerant and localized electrons, derive an expression for the torques by which the itinerant electrons act on the localized electrons and show how the static domain wall from section 2.3 will move under an applied magnetic field and electric current.

3.1 The *sd*-model of ferromagnetism

The spin-transfer torque can be understood if we distinguish between two different electron dynamics; that of the itinerant conduction electrons and that of the localized electrons [13]. That we should distinguish between these two electron dynamics can be justified by looking at the schematic density of states in

Figure 3.1 which is valid for ferromagnetic transition metals [36]. Although it is impossible to unambiguously separate the itinerant and the localized electrons in a real ferromagnet, the two dynamics have conventionally been modeled using the *sd*-model.

The current is carried by the electrons at the Fermi level. The *d*-electrons have flat bands and correspondingly large effective masses that prevent them from participating in transport. As a result, transport is entirely ascribed to the *s*-electrons. On the other hand, it is the spin-dependence of the density of states of the *d*-electrons that is responsible for the local magnetization. The spin polarization of the *s*-electrons that carry the current couples to the local magnetization through the *sd* exchange interaction,

$$\widehat{H}_{sd} = -J_{\mathrm{ex}}\widehat{\boldsymbol{s}} \cdot \widehat{\boldsymbol{S}}, \tag{3.1}$$

where $\widehat{\boldsymbol{s}}$ and $\widehat{\boldsymbol{S}}$ are the (dimensionless) spin operators of the itinerant *s*-electrons and the localized *d*-electrons, respectively.

3.2 Spin-transfer torques

Berger (1978) was the first to consider spin-transfer torques [42, 43]. However, there was no widespread interest in this field until the discovery of the GMR effect by Grünberg and Fert in 1988 had attracted attention to magnetic nanostructures [4, 44, 45]. The study of spin-transfer torques accelerated in 1996 when Berger and Slonczewski independently predicted that a current flowing perpendicular to a metallic multilayer stack can generate a spin-transfer torque that is able to reorient

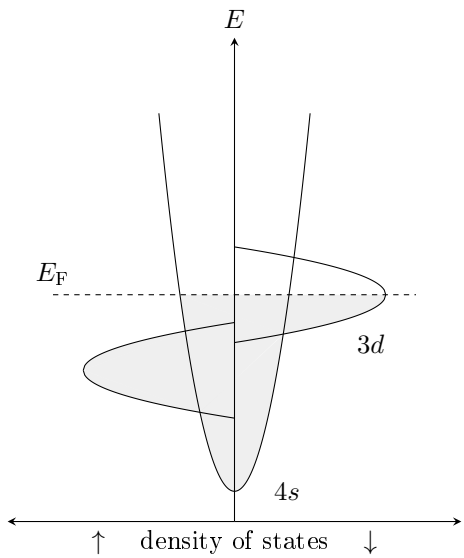

Figure 3.1: Schematic density of states for the ferromagnetic transition metals.

the magnetization in one of the layers [46, 47]. In 2004 Zhang and Li [13] gave a comprehensive treatment of the spin-transfer torque and included in addition to the adiabatic torque also the non-adiabatic torque. Our presentation of the spin-transfer torque will follow their approach.

We use the *sd*-model. The itinerant electron spin operator $\widehat{\boldsymbol{s}}$ will be treated as a full quantum mechanical operator, but the localized electron spin operator will be approximated by a classical magnetization vector $\boldsymbol{m}/m = -\boldsymbol{S}/S$—just as was done in section 2.1. This gives the *sd* Hamiltonian

$$\widehat{H}_{sd} = \frac{SJ_{\text{ex}}}{m}\widehat{\boldsymbol{s}} \cdot \boldsymbol{m}. \tag{3.2}$$

First, the induced spin density $\boldsymbol{\mu}(\boldsymbol{r},t) = \langle \boldsymbol{s} \rangle$ is determined for a given $\boldsymbol{m}(\boldsymbol{r},t)$ and then the spin torque from this spin density on $\boldsymbol{m}(\boldsymbol{r},t)$ is determined. As before, $\langle \cdots \rangle$ represents the expectation value using appropriate quantum states or a density matrix.

Back in section 2.1 we used the equation of motion for an expectation value in the Schrödinger picture (2.2). A similar equation is valid for the operator in the Heisenberg picture, named the Heisenberg equation of motion [30]. Taking into account that the spin current may act as a source or a sink of spin angular momentum and that spin relaxation need not take place by *sd* exchange we arrive at the generalized spin continuity equation

$$\partial_t \widehat{\boldsymbol{s}} + \nabla \cdot \widehat{J} = \frac{i}{\hbar}[\widehat{H}_{sd}, \widehat{\boldsymbol{s}}] - \boldsymbol{\Gamma}(\widehat{\boldsymbol{s}}) \tag{3.3}$$

for the itinerant electrons. Here, $\widehat{J}$ is the spin current density operator and $\boldsymbol{\Gamma}(\widehat{\boldsymbol{s}})$ represents spin relaxation by mechanisms other than the *sd* exchange (*e.g.* scattering with impurities, electrons, *etc.*). Define now the spin current density as the expectation value of the spin current density operator, $\mathcal{J} = \langle J \rangle$. Taking the expectation value of (3.3) we then get

$$\partial_t \boldsymbol{\mu} + \nabla \cdot \mathcal{J} = -\frac{1}{\tau_{\text{ex}} m}\boldsymbol{\mu} \times \boldsymbol{m}(\boldsymbol{r},t) - \langle \boldsymbol{\Gamma}(\widehat{\boldsymbol{s}}) \rangle, \tag{3.4}$$

where we used the trick from section 2.1 to evaluate the commutator and defined the exchange relaxation time $\tau_{\text{ex}} = \hbar/SJ_{\text{ex}}$.

We have identified the *sd* exchange as the mechanism that couples the induced spin density $\boldsymbol{\mu}$ to the magnetization $\boldsymbol{m}(\boldsymbol{r},t)$. If the *sd* exchange was the only interaction to generate the induced spin density then $\boldsymbol{\mu}(\boldsymbol{r},t)$ would follow $\boldsymbol{m}(\boldsymbol{r},t)$ adiabatically since the dynamics of the magnetization is slow compared to the dynamics of the conduction electrons. However, there are also other processes—such as scattering with impurities and with electrons—that are important to the generation of the induced spin density. Thus, we separate the induced spin density into two terms,

$$\boldsymbol{\mu}(\boldsymbol{r},t) = \boldsymbol{\mu}_0(\boldsymbol{r},t) + \delta\boldsymbol{\mu}(\boldsymbol{r},t) = n\frac{\boldsymbol{m}(\boldsymbol{r},t)}{m} + \delta\boldsymbol{\mu}(\boldsymbol{r},t), \tag{3.5}$$

where $\boldsymbol{\mu}_0$ is the equilibrium spin density which follows the magnetization adiabatically and $\delta\boldsymbol{\mu}$ is the deviation from the adiabatic process. Similarly, we write the spin current density as a sum of two terms,

$$\mathcal{J}(\boldsymbol{r},t) = \mathcal{J}_0(\boldsymbol{r},t) + \delta\mathcal{J}(\boldsymbol{r},t) = -\frac{\mu_{\mathrm{B}} P \boldsymbol{j}_e}{e} \otimes \frac{\boldsymbol{m}(\boldsymbol{r},t)}{m} + \delta\mathcal{J}(\boldsymbol{r},t), \tag{3.6}$$

where $\mathcal{J}_0$ is the spin current whose polarization follows the magnetization adiabatically and $\delta\mathcal{J}$ is the deviation from the adiabatic process. μ_{B} is the Bohr magneton, e is the electron charge and P is the spin current polarization in the ferromagnet. The adiabatic spin current density is given by a tensor product between the charge current density and the local magnetization, representing the polarization process.

What we want next is to solve (3.4) for the induced spin density $\boldsymbol{\mu}(\boldsymbol{r},t)$. In order to do so we make some simplifying assumptions and approximations with the help of the definitions (3.5) and (3.6). First, we use a simple relaxation time approximation to model the relaxation term in (3.4), *viz.* $\langle \boldsymbol{\Gamma}(\widehat{\boldsymbol{s}}) \rangle = \delta\boldsymbol{\mu}(\boldsymbol{r},t)/\tau_{\mathrm{sf}}$, where τ_{sf} is the spin-flip relaxation time [22]. Second, we consider only the linear response of $\delta\boldsymbol{\mu}$ to the charge current j_e and the time derivative $\partial_t \boldsymbol{m}$. In particular, $\partial_t \delta\boldsymbol{\mu}$ will be of the order $j_e \partial_t \boldsymbol{m}$ or $\partial_t^2 \boldsymbol{m}$ and will be discarded. Third, in the semiclassical transport model the non-equilibrium spin current density will be the flux of non-equilibrium induced spin density, $\delta\mathcal{J} = -D\nabla\delta\boldsymbol{\mu}$. D is the diffusion constant. Fourth, we use charge neutrality, $\nabla \cdot \boldsymbol{j}_e = 0$. This gives

$$D\nabla^2\delta\boldsymbol{\mu} - \frac{1}{\tau_{\mathrm{ex}} m}\delta\boldsymbol{\mu} \times \boldsymbol{m} - \frac{\delta\boldsymbol{\mu}}{\tau_{\mathrm{sf}}} = \frac{n}{m}\partial_t \boldsymbol{m} - \frac{\mu_{\mathrm{B}} P}{em}(\boldsymbol{j}_e \cdot \nabla)\boldsymbol{m}. \tag{3.7}$$

Equation (3.7) says that the non-equilibrium spin density is generated by two source terms on the right-hand side: one is the temporal change in the magnetization vector and the other is the spatial change in the magnetization vector. We are interested in slowly varying magnetization textures. This permits us to simplify (3.7) using the following argument. Write the equation as

$$\nabla^2 y - y/w^2 = f(\boldsymbol{r})$$

where $w = \sqrt{D/(1/\tau_{\mathrm{sf}} + i/\tau_{\mathrm{ex}})}$, $y = \delta\mu_\upsilon \pm \delta\mu_\zeta$ and $\delta\mu_\upsilon$ and $\delta\mu_\zeta$ are the two components of $\delta\boldsymbol{\mu}$ that are perpendicular to $\boldsymbol{m}$. The solution to this equation is

$$y(\boldsymbol{r}) = \int \frac{\exp(-|\boldsymbol{r}-\boldsymbol{r}'|/w)}{4\pi|\boldsymbol{r}-\boldsymbol{r}'|} f(\boldsymbol{r}')\mathrm{d}\boldsymbol{r}'.$$

If $f(\boldsymbol{r})$ is approximately constant on the scale of w one may replace $f(\boldsymbol{r}')$ with $f(\boldsymbol{r})$ in the integral, giving the solution $y = -w^2 f(\boldsymbol{r})$. Thus we may neglect the first term in the equation for y. We conclude that if the domain wall width λ is much larger than the length scale defined by w we may neglect the first term of equation (3.7). This leaves us with an algebraic equation for $\delta\boldsymbol{\mu}$. We solve that

equation by taking the cross product with $\boldsymbol{m}$, simplify by recognizing that $\delta\boldsymbol{\mu}$ is perpendicular to $\boldsymbol{m}$ and substitute the result back into (3.7). The result is

$$\begin{aligned}\delta\boldsymbol{\mu} = \frac{\tau_{\text{ex}}}{1+\xi^2}\Big[&-\frac{\xi n}{m}\partial_t\boldsymbol{m} - \frac{n}{m^2}\boldsymbol{m}\times\partial_t\boldsymbol{m} \\ &+\frac{\mu_{\text{B}}P\xi}{em}(\boldsymbol{j}_e\cdot\nabla)\boldsymbol{m} + \frac{\mu_{\text{B}}P}{em^2}\boldsymbol{m}\times(\boldsymbol{j}_e\cdot\nabla)\boldsymbol{m}\Big],\end{aligned} \tag{3.8}$$

where $\xi = \tau_{\text{ex}}/\tau_{\text{sf}}$.

The induced spin density $\boldsymbol{\mu}(\boldsymbol{r},t)$ exerts a torque on the magnetization $\boldsymbol{m}(\boldsymbol{r},t)$. From the Hamiltonian (3.2) it can be seen that this torque is

$$\boldsymbol{\tau} = -\frac{SJ_{\text{ex}}}{\hbar m}\boldsymbol{m}\times\boldsymbol{\mu} = -\frac{1}{\tau_{\text{ex}}m}\boldsymbol{m}\times\delta\boldsymbol{\mu}. \tag{3.9}$$

By using the expression (3.8) we have obtained for the non-equilibrium spin density we conclude that the spin torque is

$$\begin{aligned}\boldsymbol{\tau} = \frac{1}{(1+\xi^2)}\Big[&-\frac{n}{m}\partial_t\boldsymbol{m} + \frac{\xi n}{m^2}\boldsymbol{m}\times\partial_t\boldsymbol{m} \\ &-\frac{\mu_{\text{B}}P}{em^3}\boldsymbol{m}\times[\boldsymbol{m}\times(\boldsymbol{j}_e\cdot\nabla)\boldsymbol{m}] - \frac{\mu_{\text{B}}P\xi}{em^2}\boldsymbol{m}\times(\boldsymbol{j}_e\cdot\nabla)\boldsymbol{m}\Big].\end{aligned} \tag{3.10}$$

There are four terms. The two former terms are due to the temporal variation of the magnetization. Remarkably, they are independent of the current. The two latter terms are due to the spatial variation of the magnetization. When adding the torque (3.10) due to a spin-polarized current to the LLG equation (2.17),

$$\partial_t\boldsymbol{m} = \gamma\boldsymbol{m}\times\boldsymbol{H} - \frac{\alpha}{m}\boldsymbol{m}\times\partial_t\boldsymbol{m},$$

the effect of the two first terms is to renormalize the gyromagnetic ratio γ and the damping parameter α. We define $\chi = (n/m)/(1+\xi^2)$. By introducing the effective gyromagnetic ratio

$$\gamma' = \gamma/(1+\chi) \tag{3.11}$$

and the effective damping parameter

$$\alpha' = (\alpha - \xi\chi)/(1+\chi) \tag{3.12}$$

the LLG equation remains on the same form. Mind that the corrections to the gyromagnetic ratio and damping parameter due to the spin torque from itinerant s-electrons are very small. Using experimental values that are typical for transition metal ferromagnets, see Table 3.1, we find that $\chi = 10^{-2}$ and $\xi\chi = 10^{-4}$. Typical damping parameters in such materials are on the order of 10^{-2}.

Since the temporal spin torques can be absorbed in the gyromagnetic ratio and the damping parameter we concentrate on the role of the spatial spin torques. The

Table 3.1: Experimental values that are typical for transition metal ferromagnets (Ni, Co and Fe) and their alloys.

parameter	value	unit
τ_{ex}	$1 \cdot 10^{-14}$	s
τ_{sf}	$1 \cdot 10^{-12}$	s
m	$6 \cdot 10^{5}$	A/m
n	$6 \cdot 10^{3}$	A/m

first of these is the (adiabatic) spin-transfer torque which describes the adiabatic alignment of the spin density of the itinerant electrons with the local magnetization. The second of these describes the mistracking of spins between the itinerant electrons and the local magnetization and is named the non-adiabatic spin-transfer torque[1]. One might be tempted to discard the non-adiabatic spin torque because it is a factor ξ smaller than the adiabatic spin torque. However, we are going to see in section 3.3 that there cannot be a finite terminal domain wall velocity in the absence of an external magnetic field unless the effect of the non-adiabatic torque is included.

There has been some controversy over the microscopic mechanism behind the non-adiabatic spin-transfer torque. Zhang and Li claims the mechanism to be spin-flip scattering. However, a term on this functional form was first introduced by Berger [51] as a consequence of the Stern-Gerlach force on the itinerant electrons by the gradient in the *sd* exchange field. Various other authors have attributed such a term to linear momentum transfer [14] or to adiabatic spin-transfer torque in the presence of Landau-Lifshitz type damping [15]. In the following, we treat the non-adiabicity constant ξ as a phenomenological parameter similar to the Gilbert damping parameter α.

3.3 A moving domain wall

We are now going to demonstrate that by adding an external field and introducing an electric current in the system it is possible to move ferromagnetic domain walls. Just as for the static solution we start out with the LLG equation, only this time we must add the torques that are exerted on the magnetization by a spin-polarized current,

$$\partial_t \boldsymbol{m} = \gamma \boldsymbol{m} \times \boldsymbol{H} - \frac{\alpha}{m} \boldsymbol{m} \times \partial_t \boldsymbol{m} - \frac{b}{m^2} \boldsymbol{m} \times (\boldsymbol{m} \times \partial_x \boldsymbol{m}) - \frac{c}{m} \boldsymbol{m} \times \partial_x \boldsymbol{m}.$$

[1] The common point of view in the literature seems to be that this is a non-adiabatic torque, although several authors have argued otherwise [48–50]. What is clear is that this term has the same functional form as the Gilbert damping term, except that the time-derivative is replaced with a spatial derivative. Therefore, this torque is also named the dissipative spin-transfer torque. Since it is always perpendicular to the adiabatic spin-transfer torque, it has also been named the perpendicular torque or the field-like torque [3].

Note that we have assumed that the direction of the current is in the x-direction, $\boldsymbol{j} = j\boldsymbol{e}_x$, and have defined $b = Pj\mu_{\mathrm{B}}/em(1+\xi^2)$ and $c = \xi b$. The field $\boldsymbol{H}$ is again understood to be the effective field in the solid. Mind also the fact that we follow the convention that $\boldsymbol{m} = \gamma \boldsymbol{S}$, giving $\gamma < 0$ and $\alpha < 0$ for systems dominated by electron spins.

The effective field is thus made up from three terms: the external magnetic field, the exchange interaction and the magnetic anisotropy,

$$\boldsymbol{H} = \boldsymbol{H}_0 + \boldsymbol{H}_{\mathrm{ex}} + \boldsymbol{H}_{\mathrm{a}}, \tag{3.13}$$

where the external field is

$$\boldsymbol{H}_0 = H_0 \boldsymbol{e}_x,$$

the exchange coupling field is given by (2.26),

$$\boldsymbol{H}_{\mathrm{ex}} = \frac{2A}{m^2}\partial_x^2 \boldsymbol{m},$$

and the anisotropy field is given by (2.30),

$$\boldsymbol{H}_{\mathrm{a}} = \frac{2K}{m^2} m_x \boldsymbol{e}_x - \frac{2K_\perp}{m^2} m_z \boldsymbol{e}_z.$$

The x-axis is the easy axis due to the contribution from the demagnetization energy and the z-axis is the hard axis—this could be a magnetocrystalline anisotropy effect.

The magnetization can be written

$$\boldsymbol{m} = m(\cos\vartheta \boldsymbol{e}_x + \cos\varphi \sin\vartheta \boldsymbol{e}_y + \sin\varphi \sin\vartheta \boldsymbol{e}_z)$$

since the LLG equation conserves the length of the magnetization vector. If this parametrization is substituted back into the LLG equation, the following terms are obtained. The external field contributes a term

$$\gamma \boldsymbol{m} \times \boldsymbol{H}_0 = \gamma m H_0 (\sin\varphi \sin\vartheta \boldsymbol{e}_y - \cos\varphi \sin\vartheta \boldsymbol{e}_z).$$

The exchange coupling contributes a term

$$\begin{aligned}
\gamma \boldsymbol{m} \times \boldsymbol{H}_{\mathrm{ex}} = 2\gamma A \Big[& \sin\vartheta \Big(2\cos\vartheta (\partial_x\varphi)(\partial_x\vartheta) + \sin\vartheta (\partial_x^2\varphi) \Big) \boldsymbol{e}_x \\
& + \Big(\sin\varphi \sin\vartheta \cos\vartheta (\partial_x\varphi)^2 - 2\cos\varphi \cos^2\vartheta (\partial_x\varphi)(\partial_x\vartheta) \\
& - \cos\varphi \sin\vartheta \cos\vartheta (\partial_x^2\varphi) - \sin\varphi (\partial_x^2\vartheta) \Big) \boldsymbol{e}_y \\
& - \Big(\cos\varphi \sin\vartheta \cos\vartheta (\partial_x\varphi)^2 + 2\sin\varphi \cos^2\vartheta (\partial_x\varphi)(\partial_x\vartheta) \\
& + \sin\varphi \sin\vartheta \cos\vartheta (\partial_x^2\varphi) - \cos\varphi (\partial_x^2\vartheta) \Big) \boldsymbol{e}_z \Big].
\end{aligned}$$

The magnetic anisotropy contributes a term

$$\gamma \boldsymbol{m} \times \boldsymbol{H}_{\mathrm{a}} = -2\gamma \Big[K_{\perp} \cos\varphi \sin\varphi \sin^2\vartheta \boldsymbol{e}_x - (K + K_{\perp}) \sin\varphi \cos\vartheta \sin\vartheta \boldsymbol{e}_y + K \cos\varphi \sin\vartheta \cos\vartheta \boldsymbol{e}_z \Big].$$

The Gilbert damping contributes a term

$$\frac{\alpha}{m} \boldsymbol{m} \times \partial_t \boldsymbol{m} = m\alpha \Big[\sin^2\vartheta (\partial_t\varphi) \boldsymbol{e}_x - \Big(\cos\varphi \cos\vartheta \sin\vartheta (\partial_t\varphi) + \sin\varphi (\partial_t\vartheta) \Big) \boldsymbol{e}_y - \Big(\sin\varphi \cos\vartheta \sin\vartheta (\partial_t\varphi) - \cos\varphi (\partial_t\vartheta) \Big) \boldsymbol{e}_z \Big].$$

The adiabatic torque contributes a term

$$\frac{b}{m^2} \boldsymbol{m} \times (\boldsymbol{m} \times \partial_x \boldsymbol{m}) = -mb \Big[\sin\vartheta (\partial_x\vartheta) \boldsymbol{e}_x + \Big(\sin\varphi \sin\vartheta (\partial_x\varphi) - \cos\varphi \cos\vartheta (\partial_x\vartheta) \Big) \boldsymbol{e}_y - \Big(\cos\varphi \sin\vartheta (\partial_x\varphi) + \sin\varphi \cos\vartheta (\partial_x\vartheta) \Big) \boldsymbol{e}_z \Big].$$

Finally, the non-adiabatic torque contributes a term

$$\frac{c}{m} \boldsymbol{m} \times \partial_x \boldsymbol{m} = -mc \Big[\sin^2\vartheta (\partial_x\varphi) \boldsymbol{e}_x - \Big(\cos\varphi \sin\vartheta \cos\vartheta (\partial_x\varphi) + \sin\varphi (\partial_x\vartheta) \Big) \boldsymbol{e}_y - \Big(\sin\varphi \sin\vartheta \cos\vartheta (\partial_x\varphi) - \cos\varphi (\partial_x\vartheta) \Big) \boldsymbol{e}_z \Big].$$

A short comment regarding the adiabatic torque term seems to be appropriate. The astute reader will notice that when we evaluate this term we find

$$\frac{b}{m^2} \boldsymbol{m} \times (\boldsymbol{m} \times \partial_x \boldsymbol{m}) = -b \partial_x \boldsymbol{m}. \tag{3.14}$$

This is not a coincidence. Since the LLG equation conserves the length of the magnetization vector, derivatives of the magnetization vector must be at right angles with the magnetization vector itself. This is a consequence of the general argument that if we take the derivative of both sides of the equation

$$\boldsymbol{m} \cdot \boldsymbol{m} = m^2$$

we get the result that the dot product is zero,

$$2\boldsymbol{m} \cdot \boldsymbol{m}' = 0. \tag{3.15}$$

(The prime denotes any derivative.) A dot product that is zero is the definition of vector orthogonality. In particular, $\boldsymbol{m} \perp \partial_x \boldsymbol{m}$, and so the combined action of the two cross products is to change $\partial_x \boldsymbol{m}$ into the anti-parallel vector, $-\partial_x \boldsymbol{m}$.

Using the expressions we have obtained for each term in the LLG equation, we can sort out the following component equations. The x-component gives

$$\begin{aligned} -\sin\vartheta (\partial_t\vartheta) = & \frac{2\gamma A}{m} \sin\vartheta \Big[2\cos\vartheta (\partial_x\varphi)(\partial_x\vartheta) + \sin\vartheta (\partial_x^2\varphi) \Big] \\ & - \frac{2\gamma K_{\perp}}{m} \cos\varphi \sin\varphi \sin^2\vartheta - \alpha \sin^2\vartheta (\partial_t\varphi) \\ & - b \sin\vartheta (\partial_x\vartheta) - c \sin^2\vartheta (\partial_x\varphi). \end{aligned} \tag{3.16}$$

The y-component gives

$$\begin{aligned}
-\sin\varphi\sin\vartheta(\partial_t\varphi)+\cos\varphi\cos\vartheta(\partial_t\vartheta) &= \gamma H_0\sin\varphi\sin\vartheta\\
&+\frac{2\gamma A}{m}\Big[\sin\varphi\sin\vartheta\cos\vartheta(\partial_x\varphi)^2-2\cos\varphi\cos^2\vartheta(\partial_x\varphi)(\partial_x\vartheta)\\
&-\cos\varphi\sin\vartheta\cos\vartheta(\partial_x^2\varphi)-\sin\varphi(\partial_x^2\vartheta)\Big]+\frac{2\gamma(K+K_\perp)}{m}\sin\varphi\cos\vartheta\sin\vartheta\\
&+\alpha\Big[\cos\varphi\cos\vartheta\sin\vartheta(\partial_t\varphi)+\sin\varphi(\partial_t\vartheta)\Big]\\
&-b\Big[\sin\varphi\sin\vartheta(\partial_x\varphi)-\cos\varphi\cos\vartheta(\partial_x\vartheta)\Big]\\
&+c\Big[\cos\varphi\sin\vartheta\cos\vartheta(\partial_x\varphi)+\sin\varphi(\partial_x\vartheta)\Big]
\end{aligned}$$

The z-component gives

$$\begin{aligned}
\cos\varphi\sin\vartheta(\partial_t\varphi)+\sin\varphi\cos\vartheta(\partial_t\vartheta) &= -\gamma H_0\cos\varphi\sin\vartheta\\
&-\frac{2\gamma A}{m}\Big[\cos\varphi\sin\vartheta\cos\vartheta(\partial_x\varphi)^2+2\sin\varphi\cos^2\vartheta(\partial_x\varphi)(\partial_x\vartheta)\\
&+\sin\varphi\sin\vartheta\cos\vartheta(\partial_x^2\varphi)-\cos\varphi(\partial_x^2\vartheta)\Big]-\frac{2\gamma K}{m}\cos\varphi\sin\vartheta\cos\vartheta\\
&+\alpha\Big[\sin\varphi\cos\vartheta\sin\vartheta(\partial_t\varphi)-\cos\varphi(\partial_t\vartheta)\Big]\\
&+b\Big[\cos\varphi\sin\vartheta(\partial_x\varphi)+\sin\varphi\cos\vartheta(\partial_x\vartheta)\Big]\\
&+c\Big[\sin\varphi\sin\vartheta\cos\vartheta(\partial_x\varphi)-\cos\varphi(\partial_x\vartheta)\Big].
\end{aligned}$$

The y- and the z-component look very similar, so we multiply the former with $\sin\varphi$ and the latter with $\cos\varphi$ and subtract the two to get

$$\begin{aligned}
-\sin\vartheta(\partial_t\varphi) =& \frac{2\gamma A}{m}\Big[\sin\vartheta\cos\vartheta(\partial_x\varphi)^2-(\partial_x^2\vartheta)\Big]\\
&+\frac{2\gamma K}{m}\sin\vartheta\cos\vartheta(1+\kappa\sin^2\varphi)\\
&+\alpha(\partial_t\vartheta)+\gamma H_0\sin\vartheta-b\sin\vartheta(\partial_x\varphi)+c(\partial_x\vartheta),
\end{aligned}\tag{3.17}$$

with $\kappa = K_\perp/K$. We have two unknown functions $\varphi(x,t)$ and $\vartheta(x,t)$, so two differential equations are sufficient for solving the system. We conclude that the x-component equation (3.16) together with (3.17) provides the equations of motion of the magnetization field. We note that since

$$\partial_x\Big[\sin^2\vartheta(\partial_x\varphi)\Big]=2\sin\vartheta\cos\vartheta(\partial_x\vartheta)(\partial_x\varphi)+\sin^2\vartheta(\partial_x^2\varphi)$$

the x-component equation (3.16) can be written as

$$\begin{aligned}
-\sin\vartheta(\partial_t\vartheta) =& \frac{2\gamma A}{m}\partial_x\Big[\sin^2\vartheta(\partial_x\varphi)\Big]-\frac{2\gamma K_\perp}{m}\cos\varphi\sin\varphi\sin^2\vartheta\\
&-\alpha\sin^2\vartheta(\partial_t\varphi)-b\sin\vartheta(\partial_x\vartheta)-c\sin^2\vartheta(\partial_x\varphi).
\end{aligned}\tag{3.18}$$

3.3.1 A first attempt to solve the equations of motion

Having obtained the equations of motion we solve them under different assumptions. Assume first that $\partial_x\varphi = \partial_t\varphi = 0$ and that $\partial_x\vartheta|_{\pm\infty} = 0$. This is the case investigated by Shibata *et al.* [5], and we are able to reproduce their results. The equations of motion are

$$-\sin\vartheta(\partial_t\vartheta) = -\frac{2\gamma K_\perp}{m}\cos\varphi\sin\varphi\sin^2\vartheta - b\sin\vartheta(\partial_x\vartheta)$$

and

$$-\alpha(\partial_t\vartheta) = -\frac{2\gamma A}{m}(\partial_x^2\vartheta) + \frac{2\gamma K}{m}\sin\vartheta\cos\vartheta(1+\kappa\sin^2\varphi) + \gamma H_0\sin\vartheta + c(\partial_x\vartheta).$$

We substitute the first into the second to find

$$\begin{aligned}-\frac{2\gamma K}{m}\sin\vartheta\Big[\lambda^2(\partial_x^2\vartheta) - \sin\vartheta\cos\vartheta(1+\kappa\sin^2\varphi)\Big]\\ = -\alpha\left[\frac{\gamma K_\perp}{m}\sin 2\varphi\sin^2\vartheta + b\sin\vartheta(\partial_x\vartheta)\right] - \sin\vartheta\Big[\gamma H_0\sin\vartheta + c(\partial_x\vartheta)\Big]\end{aligned}$$

with $\lambda = \sqrt{A/K}$. Using $\Lambda = \lambda/\sqrt{1+\kappa\sin^2\varphi}$ we can rewrite this as

$$\begin{aligned}\frac{2\gamma K}{m}\left(\frac{\lambda}{\Lambda}\right)^2\sin\vartheta\Big[\Lambda^2(\partial_x^2\vartheta) - \sin\vartheta\cos\vartheta\Big]\\ = \frac{\alpha\gamma K_\perp}{m}\sin 2\varphi\sin^2\vartheta + b(\alpha+\xi)\sin\vartheta(\partial_x\vartheta) + \gamma H_0\sin^2\vartheta\end{aligned}$$

with $c = \xi b$. We require both members of the equation to be zero simultaneously. The left-hand side then gives the familiar equation for a domain wall profile that we solved in section 2.3,

$$\Lambda^2(\partial_x^2\vartheta) = \sin\vartheta\cos\vartheta \qquad \Rightarrow \qquad \vartheta(x,t) = 2\arctan\exp\left[\pm\frac{x-X(t)}{\Lambda}\right],$$

where $X(t)$ is the integration constant which might now be time-dependent. The result of such a time-dependency is that the domain wall can travel along the x-axis, quite different from the static domain wall we obtained before. The domain wall velocity, $\dot{X} = \mathrm{d}X/\mathrm{d}t$, can be obtained by substituting the expression we have obtained for ϑ back into the equations of motion, as we are going to do below. If we use

$$\partial_x\vartheta = \pm\frac{\sin\vartheta}{\Lambda}$$

the right-hand side determines φ and gives a limit on the driving forces in the system:

$$\sin 2\varphi = \frac{m}{\alpha\gamma K_\perp}\left[\gamma H_0 \pm \frac{b}{\Lambda}(\alpha+\xi)\right] \tag{3.19}$$

and

$$\left|\frac{\alpha\gamma K_\perp}{m}\right| \geq \left|\gamma H_0 \pm \frac{b}{\Lambda}(\alpha+\xi)\right|. \tag{3.20}$$

This limit implies that our initial assumptions $\partial_x\varphi = \dot{\varphi} = 0$ are inapplicable for larger driving forces. The limit we have obtained is known as the threshold for Walker breakdown [18]. Walker breakdown is the deformation of a domain wall by the driving forces for domain wall motion—in this case current and field. Since the objective of domain wall transport is to use the domain walls to represent information domain walls should not be deformed or destroyed by our manipulations. In particular, devices that make use of domain wall transport should stay below the threshold for Walker breakdown.

3.3.2 Solving the equations of motion using Walker's *ansatz*. Collective coordinates

Using the assumptions $\partial_x\varphi = \partial_t\varphi = 0$ we arrived at a domain wall traveling in the x-direction. In order to determine the domain wall velocity we substitute this solution back into the equations of motion. That is, relax the assumption that $\dot{\varphi} = 0$, giving

$$\varphi = \varphi(t),$$

but use instead Walker's *ansatz* [18]

$$\vartheta(x,t) = 2\arctan\exp\left[\frac{x - X(t)}{W(t)}\right]$$

and, as before, $\partial_x\varphi = 0$. Our initial conditions are that $\varphi(0) = 0$, $X(0) = 0$ and $W(0) = \lambda$, so we are using a domain wall with positive topological charge and positive chirality, see Figure 3.2. This is the case investigated by Li and Zhang [11], and we are able to reproduce their results below.

The equations we have set up describe the domain wall in terms of three time-dependent coordinates (X, W, φ), effectively treating the domain wall as a quasi-particle with three degrees of freedom: translation, rotation and size. However,

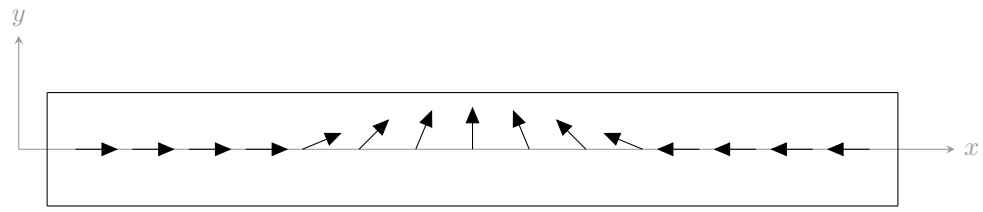

Figure 3.2: A domain wall with a positive topological charge and a positive chirality.

the domain wall is made up from a large number of spins, comprising a much larger number of degrees of freedom. The procedure of reducing the number of independent variables is named the collective coordinate method, and is discussed more thoroughly by Shibata *et al.* [5].

Before we write out the equations of motion we need to evaluate the derivatives of ϑ. We know from the solution of the equation for the domain wall profile that

$$\partial_x \vartheta = \frac{\sin\vartheta}{W}. \tag{3.21}$$

Using this equation we can evaluate the second spatial derivative,

$$\partial_x^2 \vartheta = \frac{\partial_x \sin\vartheta}{W} = \frac{\cos\vartheta(\partial_x\vartheta)}{W} = \frac{\sin\vartheta\cos\vartheta}{W^2}. \tag{3.22}$$

All that remains is the time-derivative. To obtain a useful expression for the time-derivative we need to develop a computational trick. We have assumed that the domain wall can be described by a solution on the form

$$\tan\tfrac{1}{2}\vartheta = \exp\left[\frac{x - X(t)}{W(t)}\right].$$

This solution can also be rewritten in terms of the hyperbolic functions. We write

$$\tan\tfrac{1}{2}\vartheta = \frac{\sin\frac{1}{2}\vartheta}{\cos\frac{1}{2}\vartheta} = \sqrt{\frac{1-\cos\vartheta}{1+\cos\vartheta}} = \exp\left[\frac{x - X(t)}{W(t)}\right]$$

using a trigonometric identity for sines and cosines of semi-angles. Solving for $\cos\vartheta$ we find that

$$\cos\vartheta = \frac{\exp(2[x - X(t)]/\lambda) - 1}{\exp(2[x - X(t)]/\lambda) + 1} = \tanh\left[\frac{x - X(t)}{W(t)}\right]. \tag{3.23}$$

By using $\cos^2\vartheta + \sin^2\vartheta = 1$ we may also solve for $\sin\vartheta$ to get

$$\sin\vartheta = \operatorname{sech}([x - X(t)]/\lambda). \tag{3.24}$$

Evaluating the time-derivative we obtain

$$\partial_t\vartheta = -\frac{2\exp([x - X(t)]/W(t))}{W(t)[1 + \exp(2[x - X(t)]/W(t))]}\left[\dot{X} + \frac{\dot{W}}{W}(x - X)\right].$$

Using (3.24) we see that this is the same as

$$\partial_t\vartheta = -\frac{\sin\vartheta}{W}\left[\dot{X} + \frac{\dot{W}}{W}(x - X)\right]. \tag{3.25}$$

Our equations of motion are then

$$\frac{\sin^2\vartheta}{W}\left[\dot{X} + \frac{\dot{W}}{W}(x - X)\right] = -\frac{\gamma K_\perp}{m}\sin 2\varphi\sin^2\vartheta - \alpha\sin^2\vartheta\dot{\varphi} - \frac{b}{W}\sin^2\vartheta$$

and

$$-\sin\vartheta\dot{\varphi} = -\frac{2\gamma A}{mW^2}\sin\vartheta\cos\vartheta + \frac{2\gamma K}{m}\sin\vartheta\cos\vartheta(1+\kappa\sin^2\varphi) - \frac{\alpha\sin\vartheta}{W}\left[\dot{X} + \frac{\dot{W}}{W}(x-X)\right] + \gamma H_0\sin\vartheta + \frac{c}{W}\sin\vartheta.$$

We integrate out the x-dependence from these equations by using that $\sin\vartheta$ is an even function of x while $\cos\vartheta$ and $(x-X)/W$ are odd functions of x; all symmetries about the same point $x = X/W$. The resulting equations of motion in collective coordinates are

$$\frac{\dot{X}}{W} + \alpha\dot{\varphi} = -\frac{\gamma K_\perp}{m}\sin 2\varphi - \frac{b}{W} \tag{3.26}$$

and

$$\frac{\alpha\dot{X}}{W} - \dot{\varphi} = \gamma H_0 + \frac{c}{W}. \tag{3.27}$$

These two differential equations determine the functions X and φ, but another equation is needed in order to determine W. We obtain this equation from the second equation of motion. We assume that

$$\left|\dot{X}\right| \gg \left|\frac{\dot{W}}{W}(x-X)\right|.$$

The smallness of this term cannot be ascertained *a priori*, but is confirmed numerically [11]. Then, if we compare the two versions of the second equation of motion before and after the x-dependence has been removed, we must conclude that

$$\frac{2\gamma K}{m}\left[\left(\frac{\lambda}{W}\right)^2 - (1+\kappa\sin^2\varphi)\right] = 0,$$

which is an algebraic equation for W. Solving this equation we find that W is in fact equal to the wall width Λ we found before, a result that should not be very surprising.

The equations of motion (3.26) and (3.27) contain derivatives of both φ and X. By multiplying (3.26) with α and subtracting the equations we obtain

$$(1+\alpha^2)\dot{\varphi} = -\frac{\alpha\gamma K_\perp}{m}\sin 2\varphi - \gamma H_0 - \frac{b}{\lambda}\sqrt{1+\kappa\sin^2\varphi}(\alpha+\xi). \tag{3.28}$$

By multiplying (3.27) with α and adding the equations we obtain

$$(1+\alpha^2)\frac{\dot{X}}{\Lambda} = -\frac{\gamma K_\perp}{m}\sin 2\varphi + \alpha\gamma H_0 - \frac{b}{\Lambda}(1-\xi\alpha). \tag{3.29}$$

The former equation alone can be used to determine $\varphi(t)$, but the latter equation can only be used to determine $X(t)$ once $\varphi(t)$ is known. Thus we solve (3.28) first. We observe that by setting $\dot{\varphi} = 0$ we can determine the critical threshold for Walker breakdown by reproducing (3.20). Just as we found above, φ is given by (3.19) in the subcritical regime. Note that since our initial condition is $\varphi(0) = 0$ the function $\varphi(t)$ must exhibit some brief transient behavior to reach a finite angle, thus reversibly tilting and contracting the wall.

In the subcritical regime the domain wall velocity is

$$\dot{X} = \frac{W}{\alpha}\left(\gamma H_0 + \frac{c}{W}\right). \tag{3.30}$$

Remember that our convention is $\gamma < 0$ and $\alpha < 0$. It is easy to see that the above expression for $\dot{X}$ is correct. Consider the first term, which is due to the external magnetic field. An externally applied field in the x-direction generates a torque on the spins in the wall that cants them an angle φ out of the plane, as shown in Figure 3.3. When φ is no longer zero the spins also feel a torque arising from the hard axis anisotropy which rotates them about the z-axis, producing domain wall translation [5, 20]. Walker breakdown takes place if the external field is strong enough to overcome the anisotropy field and drive the domain wall plane into precession.

Consider the second term, which is due to the current. Looking at Figure 3.2 it is clear that when there is a current to the right—*i.e.* electrons moving to the left—the the spin-transfer mechanism will cause the wall to move to the left. The expression for $\dot{X}$ also emphasizes the critical role of the non-adiabatic spin-transfer torque. In the absence of an external magnetic field the adiabatic torque alone is

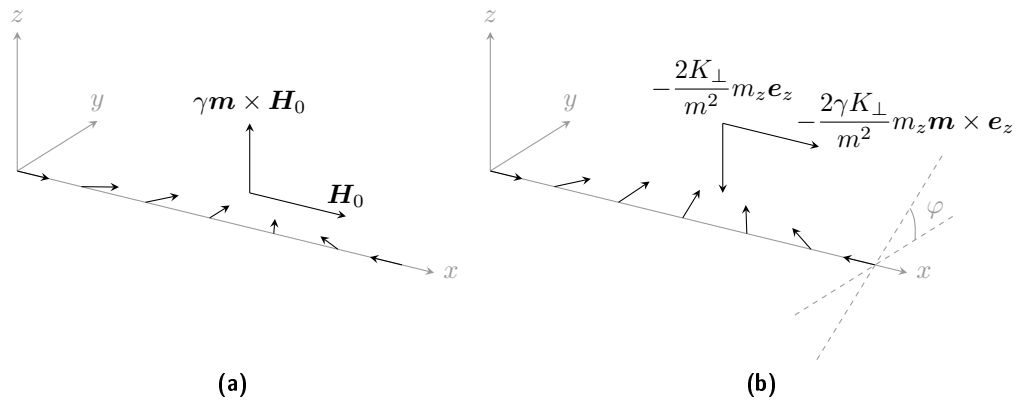

Figure 3.3: The mechanism of field induced domain wall translation for subcritical fields. (a) The external field acts with a torque that cants the spins at an angle φ out of the equilibrium position; (b) This induces a torque from the hard axis anisotropy that rotates the spins into alignment with the external field. Redrawn after reference [20].

unable to sustain a finite terminal domain wall velocity.

In the supercritical regime the condition $\dot{\varphi} = 0$ does not hold, and we must solve the full equation (3.28). This equation is hard to solve, and we make the common assumption that $\kappa \ll 1$ to make the equation tractable. Incidentally, this assumption also ensures that the collective coordinate approach is valid [5] and is easy to realize experimentally using nanowires made from soft magnetic materials such as permalloy [20]. In this regime, the equation for $\varphi(t)$ is on the general form

$$A\frac{\mathrm{d}y}{\mathrm{d}x} = -B\sin 2y + C.$$

We can solve it by separating the variables, giving

$$\frac{A\mathrm{d}y}{C - B\sin 2y} = \mathrm{d}x.$$

The integration of the right-hand side is trivial. By using a tabulated integral the left-hand side gives

$$\int \frac{A\mathrm{d}y}{C - B\sin 2y} = -\frac{A}{\sqrt{C^2 - B^2}} \arctan \frac{B - C\tan y}{\sqrt{C^2 - B^2}},$$

as can be verified by differentiation. Equating the right-hand and the left-hand sides gives finally

$$y(x) = \arctan\left[\frac{1}{C}\sqrt{C^2 - B^2}\tan\left[\sqrt{C^2 - B^2}\left(\frac{x}{A} + k\right)\right] + \frac{B}{C}\right]$$

provided that $C \neq 0$ and $|C| > |B|$. Of course, A must fulfill $A \neq 0$ or else we are back at the case $\dot{\varphi} = 0$. k is the constant of integration and is determined by the initial value $\varphi(0) = 0$. It is clear that this solution has a periodicity of $\pi A/\sqrt{C^2 - B^2}$ which is passed down to $y'(x)$. Both functions are plotted in Figure 3.4.

For comparison with experiments, the functions $\varphi(t)$ and $X(t)$ themselves are not very useful do to their oscillating behavior. Instead, we are interested in time-averaged values $\langle\dot{\varphi}\rangle$ and $\langle\dot{X}\rangle$ which are easy to compare with average velocities obtained experimentally. To obtain the time-averaged value $\langle y'\rangle$ we thus integrate y' over one period and divide by the length of the period. We may neglect the constant k due to the periodicity of $y(x)$. The integration is trivial since

$$\langle y'\rangle = \frac{1}{2a}\int_{-a}^{+a} y'(x)\mathrm{d}x = y(+a) - y(-a).$$

By letting $a \to \pi A/2\sqrt{C^2 - B^2}$ we find

$$A\langle y'\rangle = \sqrt{C^2 - B^2}$$

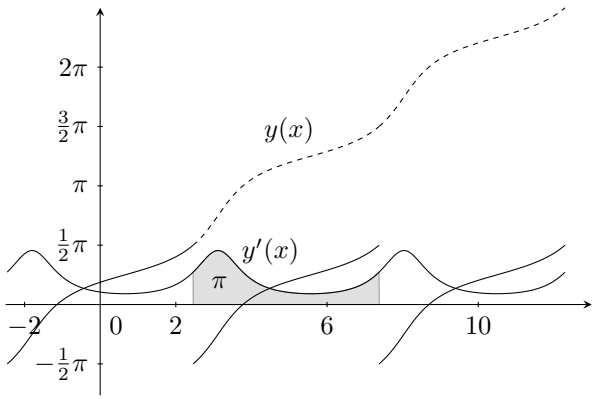

Figure 3.4: The functions $y(x)$ and $y'(x)$ for $A = 1.75$, $B = 1$ and $C = 1.5$. We have taken $k = 0$. The function $y(t)$ shows periodic discontinuities because only the principal values of the arctangent are plotted, but the derivative $\dot{\varphi}(t)$ is continuous and the physical interpretation must be that the angle φ increases steadily with time as indicated by the dashed line. The periodicity of $\dot{\varphi}(t)$ corresponds to the motion of $\boldsymbol{m}$ through the hard axis.

since $\lim_{x\to\infty} \arctan x = \pi/2$ as can also be seen from Figure 2.3. This gives the supercritical solution

$$(1+\alpha^2)\langle\dot{\varphi}\rangle = \sqrt{\left[\frac{b}{\lambda}(\xi+\alpha)+\gamma H_0\right]^2 - \left[\frac{\alpha\gamma K_\perp}{m}\right]^2}. \tag{3.31}$$

Since we are interested in the time-averaged domain wall velocity it is not necessary to solve (3.29), we just use (3.27) to find

$$\frac{\langle\dot{X}\rangle}{\lambda} - \frac{\langle\dot{\varphi}\rangle}{\alpha} = \frac{\gamma H_0}{\alpha} + \frac{\xi b}{\alpha\lambda}. \tag{3.32}$$

In the supercritical regime, the mechanism for field induced motion described above breaks down, and this is the reason why we initially observe a decrease in domain wall velocity when the field strength increases beyond the Walker limit. With increasing field the precession of the wall plane becomes more rapid, leading to a small damping torque that drives the wall translation. According to Beach *et al.* [20] it is this damping torque that provides the dominant net contribution to the wall velocity at high fields.

As can be seen from comparing the expressions for the domain wall velocity in the subcritical (3.30) and supercritical (3.29) regimes there is also a change in the mechanism of current induced translation when going from the subcritical to the supercritical regime. While the non-adiabatic torque is solely responsible for the terminal domain wall velocity in the subcritical regime, the adiabatic torque is the main contributor to the net wall velocity in the supercritical regime. It dominates the non-adiabatic torque by a factor $1/\xi\alpha$.

3.3.3 Current-driven wall motion: a special case

It is evident that for the current-driven case, $H_0 = 0$, the value $\xi = -\alpha$ is some sort of critical value. When $\xi = -\alpha$ we have

$$(1+\alpha^2)\frac{\mathrm{d}\varphi}{\mathrm{d}t} = -\frac{\alpha\gamma K_\perp}{m}\sin 2\varphi$$

and it is easy to separate the variables and integrate the equation:

$$\varphi(t) = \arctan\exp\left[-\frac{2\alpha}{1+\alpha^2}\frac{\gamma K_\perp}{m}t + k\right],$$

where we used the tabulated integral (2.40). k is the constant of integration, which is not the same constant as used above. This constant is determined by the initial condition $\varphi(0) = 0$. We know the behavior of the solution $\varphi(t)$ from the solution of the static wall problem in section 2.3, see Figure 2.3, and it is easy to see that the initial condition forces $k \to \infty$. In that case the derivative $\dot{\varphi}$ vanishes, $\dot{\varphi} \to 0$, and we can see from equation (3.29) that the wall moves at a constant rate $\dot{X} = -b$.

It is difficult to interpret the physical significance of the critical value $\xi = -\alpha$. Both the Gilbert damping term and the non-adiabatic torque are dissipative terms. It follows that the ratio ξ/α is a measure of the relative time scales of the relaxation of the induced spin density (magnetization) towards the local magnetization (effective field), although a more detailed treatment depends on the microscopic mechanism responsible for the non-adiabatic torque. But it is easy to see from the solution that when $\xi = -\alpha$ and $H_0 = 0$ there is no Walker breakdown because $\dot{\varphi} = 0$ for all values of j. For $\xi = -\alpha$, then, the domain wall is not deformed. For $\xi > -\alpha$ domain wall deformation slows down the wall, while for $\xi < -\alpha$ domain wall deformation accelerates the wall.

3.3.4 The effect of damping on domain wall behavior

Let us now consider the domain wall velocities we have obtained from the perspective of damping strength, and let us do this for field-driven motion only. If we neglect the variable wall width in the expressions for the wall velocity we have

$$\dot{X} = \frac{\lambda\gamma H_0}{\alpha}$$

for subcritical fields, see equation (3.30). For supercritical fields we have an expression

$$\dot{X} = -\frac{\lambda\gamma K_\perp}{m(1+\alpha^2)}\sin 2\varphi + \frac{\alpha\lambda\gamma H_0}{1+\alpha^2},$$

see equation (3.29). In the limit where the damping is exceedingly large, $\alpha \to \infty$, the domain wall is stationary is both cases. This should not come as a surprise—a finite field value means that there is only a finite Zeeman energy award related

to moving the wall, while the damping term is able to absorb an infinite amount of energy. In the limit where the damping is very small, $\alpha \to 0$, the supercritcal solution is still well-behaved. $\dot{\varphi} = -\gamma H_0/(1+\alpha^2)$ in this case and the domain wall performs oscillatory motion synchronized with breathing, *i.e.* domain wall extension and contraction. The subcritical solution tends to infinity, which is clearly nonsense. This nonsensical behavior is a result of our previous assumptions that the deformation of the domain wall is limited to rotation of the wall plane and wall extension and contraction. A numerical investigation has been performed in this case by Wang *et al.* [52], and they find that at subcritical fields the domain wall travels at a finite velocity. The mechanism behind such a finite velocity is emission of spin-waves. At supercritical fields the domain wall does indeed perform an oscillatory motion synchronized with breathing, but this is accompanied by weak emission of spin-waves which gives a small net velocity.

3.3.5 Solving the collective coordinate equations numerically

Using the experimental values that are found in Table 3.2, which are typical for iron-nickel alloys (permalloys), we can integrate the equations (3.28) and (3.29) numerically as explained in Appendix A.

As for the results, consider first the time-dependence of φ, X and W in the subcritical regime, which is plotted in Figure 3.5a, 3.5c and 3.5e. As mentioned above, the initial value of φ is $\varphi(0) = 0$, but when field or current is applied φ stabilizes at a finite angle given by (3.19). The result is a brief transient lasting for about 75 ns. The qualitative behavior is similar for current and field, but the driving current has been chosen to be slightly more critical than the driving field to let the curves be offset for better visibility. Note how the canting of the wall plane induces domain wall contraction because a finite magnetization component is introduced along the hard axis. However, the interesting part of the subcritical behavior is the curvature of the displacement $X(t)$. Since the domain wall has a positive topological charge a magnetic field applied in the x-direction gives wall displacement in the x-direction, but since the charge carriers have a negative charge a current applied in the x-direction gives wall displacement in the negative x-direction, *cf.* equation (3.30). For the field-driven wall the initial

Table 3.2: Experimental values that are typical for permalloys.

parameter	value	unit
$\gamma \cdot (2m_e/e)$	-2.1	1
α	-0.01	1
P	0.4	1
A	$1 \cdot 10^{-11}$	J/m
m	$6 \cdot 10^5$	A/m
K	$3 \cdot 10^4$	J/m^3
$K_\perp$	$1 \cdot 10^4$	J/m^3

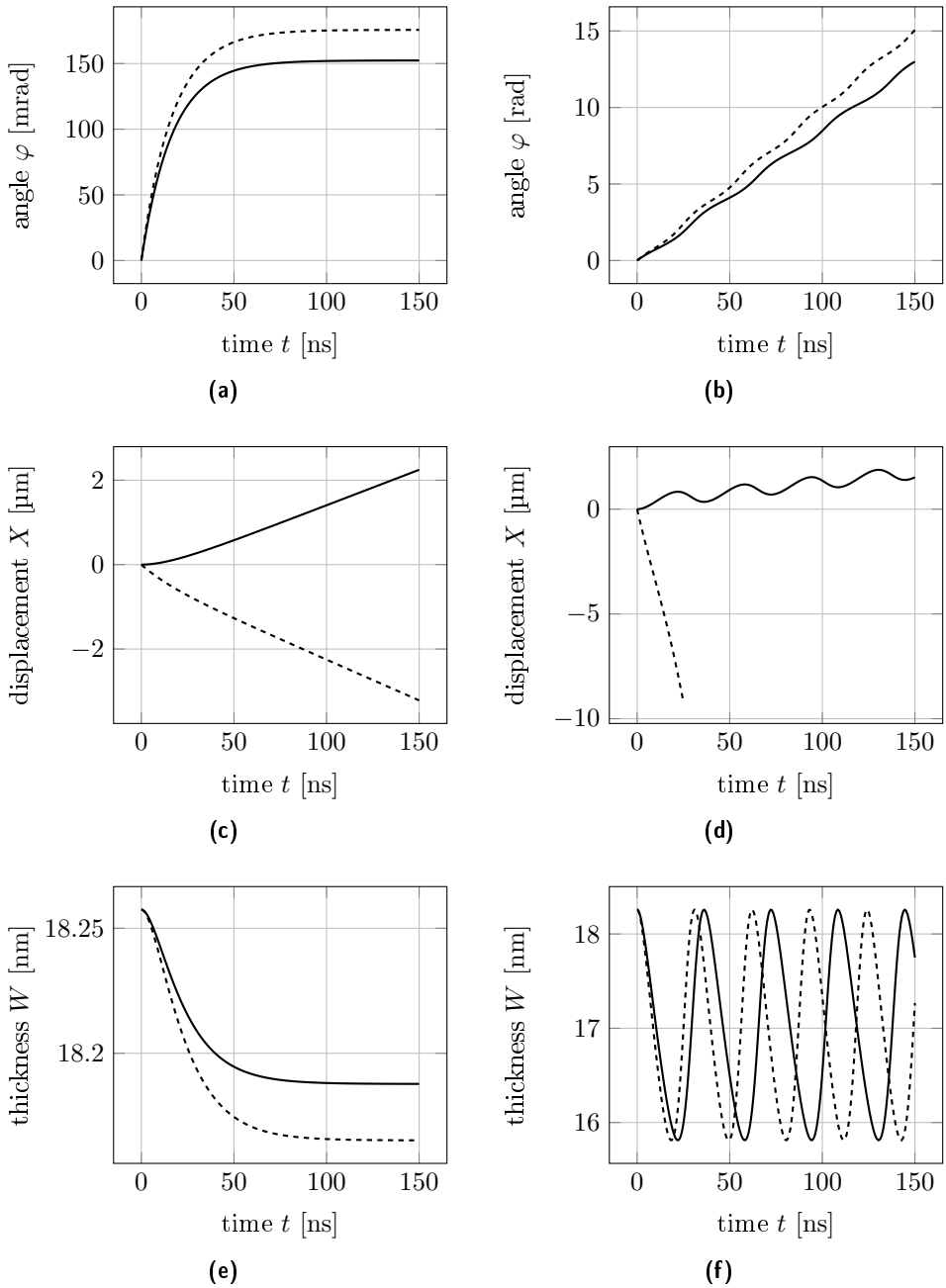

Figure 3.5: Plots of $\varphi(t)$ [panels (a) and (b)], $X(t)$ [panels (c) and (d)] and $W(t)$ [panels (e) and (f)] for experimental values that are typical for permalloys, $\xi = -\frac{1}{2}\alpha$. Possible values of ξ are discussed below. Panels (a), (c) and (e) show subcritical behavior and panels (b), (d) and (f) show supercritical behavior. Field-driven motion is plotted with solid lines and current-driven motion is plotted with dashed lines. Driving field is 0.05 mT (subcritical) and 0.5 mT (supercritical). Driving current is $100\,\mathrm{MA/cm^2}$ (subcritical) and $1\,\mathrm{GA/cm^2}$ (supercritical).

displacement is small because the spins need to be canted out of the plane at an appreciable angle before the hard axis anisotropy torque can make its contribution to wall displacement. Hence, the field-driven displacement graph has a positive curvature. For the current-driven wall the initial displacement is large because both the adiabatic and the non-adiabatic torques contribute. Only when the wall has reached its terminal distortion does it reach its terminal velocity, to which the adiabatic torque does not contribute. Hence, the current-driven displacement graph has a positive curvature too. The consequence of this is that the initial displacement of the wall is larger in the current-driven case—even at comparable criticality—possibly leading to faster domain wall manipulation. However, since the domain wall displacement resulting from the adiabatic torque is reversible [11], the curvature advantage of the current-driven wall at the initial stage of the displacement is lost when the current is switched off. Nonetheless, the curvature disadvantage of the field-driven wall remains.

Consider next the time-dependence of φ, X and W in the supercritical regime, plotted in Figure 3.5b, 3.5d and 3.5f. Still $\varphi(0) = 0$, but the driving forces are strong enough to bring the wall plane into precession and $\varphi(t)$ increases monotonically. The periodicity of $\varphi(t)$ corresponds to the motion of $\boldsymbol{m}$ through the hard axis. When φ is steadily increasing, the wall thickness starts to oscillate; this is the breathing mode. The breathing is synchronized with oscillations in the domain wall velocity. As can easily be seen from (3.29) the velocity of both the field-driven and the current-driven wall is a superposition of two terms: a linear term and an oscillating term due to the precession of φ. The velocity oscillations translates to an oscillating displacement curve, both in the case of field-driven and current-driven motion. However, the difference in scale of the linear terms ($\alpha\gamma H_0 \approx 9 \cdot 10^5$ Hz and $b/\lambda \approx 2 \cdot 10^{10}$ Hz) makes the oscillations more pronounced in the case of field-driven behavior.

Finally, consider the time averages $\langle\dot{\varphi}\rangle$ and $\langle\dot{X}\rangle$ as a function of current. We set $H_0 = 0$ since it can be seen from equation (3.31) that for averages the case of field-driven motion is similar to the case of current-driven motion with $\xi > -\alpha$. Most authors believe that ξ and α are of the same order of magnitude [48, 53–55], and we thus plot $\langle\dot{\varphi}\rangle$ and $\langle\dot{X}\rangle$ for values ξ both above and below $-\alpha$ since the behavior in these regimes is qualitatively different. The resulting plots are found in Figure 3.6a and 3.6b. For subcritical currents the average velocity is zero at large times for $\xi = 0$ as there is no non-adiabatic torque. As ξ increases, so does the velocity. The critical current depends on the value of ξ. For $\xi < -\alpha$ the velocity increases when the wall plane is driven into precession because of the additional contribution from the adiabatic torque. When $\xi > -\alpha$ we enter the regime where $(1 - \xi\alpha) > (1 + \alpha^2)$ and the velocity initially decreases with current in the supercritical regime. $\xi > -\alpha$ also corresponds to field-driven behavior, and in the field driven case the negative differential velocity is readily explained by the initiation of domain wall oscillations. Only for much larger driving fields does the contribution from the damping term compensate for the oscillations giving a net increase in velocity from the Walker breakdown velocity. We observe that for

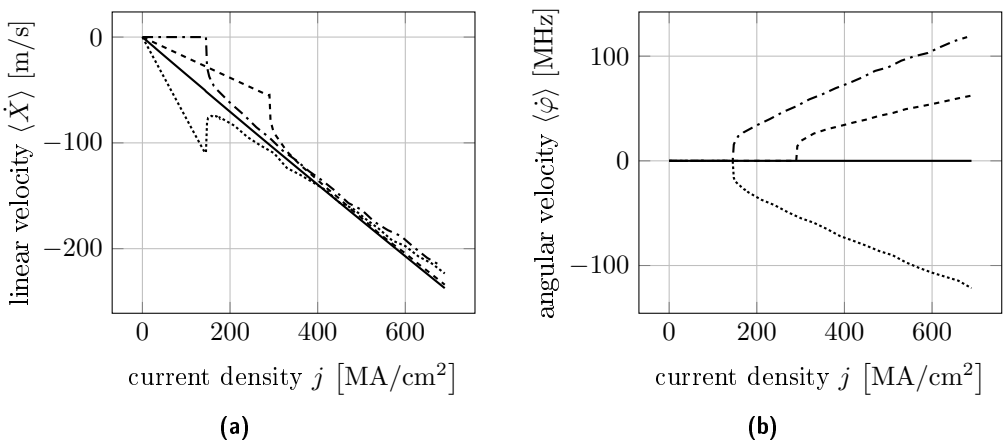

Figure 3.6: Plots of (a) $\langle \dot{\varphi} \rangle$ and (b) $\langle \dot{X} \rangle$ as functions of current density for experimental values that are typical for permalloys. The four different curves corresponds to the cases where $\xi = 0$ (–·), $\xi = -\frac{1}{2}\alpha$ (---), $\xi = -2\alpha$ (····) and $\xi = -\alpha$ (—).

large driving currents the domain wall velocity converges to $\langle \dot{X} \rangle = -b$.

3.3.6 An all-numerical solution of the LLG equation

The collective coordinate equations are a set of two coupled linear ODEs. Solving these equations numerically is relatively simple. But to obtain the equations, we had to do a considerable—though not terrifying—amount of analytical work. On the other hand, it is possible to implement a numerical solution of the LLG equation right away, without doing any analytical work at all. However, the resulting set of three coupled non-linear PDEs is much harder to solve numerically. Numerical integration of PDEs is explained in Appendix B. In the current section, we consider field-driven motion only.

To solve the LLG equation using finite difference methods we must recast the implicit Landau-Lifshitz-Gilbert (LLG) form into the explicit Landau-Lifshitz (LL) form:

$$\partial_t \boldsymbol{m} = \gamma \boldsymbol{m} \times \boldsymbol{H} - \frac{\alpha}{m} \boldsymbol{m} \times \partial_t \boldsymbol{m}.$$

We take the cross product with $\boldsymbol{m}$ from the left to get

$$\boldsymbol{m} \times \partial_t \boldsymbol{m} = \gamma \boldsymbol{m} \times (\boldsymbol{m} \times \boldsymbol{H}) - \frac{\alpha}{m} \boldsymbol{m} \times (\boldsymbol{m} \times \partial_t \boldsymbol{m}).$$

The double cross product involving $\partial_t \boldsymbol{m}$ on the right-hand side can be rewritten using the vector identity

$$\boldsymbol{a} \times (\boldsymbol{b} \times \boldsymbol{c}) = (\boldsymbol{a} \cdot \boldsymbol{c})\boldsymbol{b} - (\boldsymbol{a} \cdot \boldsymbol{b})\boldsymbol{c}.$$

We get

$$\boldsymbol{m} \times (\boldsymbol{m} \times \partial_t \boldsymbol{m}) = (\boldsymbol{m} \cdot \partial_t \boldsymbol{m})\boldsymbol{m} - (\boldsymbol{m} \cdot \boldsymbol{m})\partial_t \boldsymbol{m} = -m^2 \partial_t \boldsymbol{m}$$

by using the derivative orthogonality pointed out in (3.15). Back substitution gives

$$\begin{aligned}
\partial_t \boldsymbol{m} =& \gamma \boldsymbol{m} \times \boldsymbol{H} - \frac{\alpha}{m} \boldsymbol{m} \times \partial_t \boldsymbol{m} \\
=& \gamma \boldsymbol{m} \times \boldsymbol{H} - \frac{\alpha}{m} \Big[\gamma \boldsymbol{m} \times (\boldsymbol{m} \times \boldsymbol{H}) + m\alpha \partial_t \boldsymbol{m} \Big] \\
=& \gamma \boldsymbol{m} \times \Big[\boldsymbol{H} - \frac{\alpha}{m} \boldsymbol{m} \times \boldsymbol{H} \Big] - \alpha^2 \partial_t \boldsymbol{m}.
\end{aligned}$$

By moving all time-derivatives to the left-hand side we get

$$\partial_t \boldsymbol{m} = \frac{\gamma}{1+\alpha^2} \boldsymbol{m} \times \Big[\boldsymbol{H} - \frac{\alpha}{m} \boldsymbol{m} \times \boldsymbol{H} \Big], \tag{3.33}$$

which is the Landau-Lifshitz form. Note that we have neglected any spin-transfer torque terms.

As pointed out in subsection 3.3.4 field-driven domain walls emit spin-waves [52, 56]. To avoid spin-wave interference by reflection at the sample ends non-reflection boundary conditions should be implemented by locally increasing the Gilbert damping parameter α. According to the results of Seo *et al.* [57] such absorbing boundary conditions (ABC) are effective regardless of whether the damping constant is increased smoothly or in a single step as long as the final value of α is two orders of magnitude larger than the intrinsic value.

We use values that are typical for permalloy, see Table 3.2, and a spatial grid with length 1.2 µm and grid points spaced 1.24 nm apart. The initial profile is the Walker solution $\vartheta(x) = 2 \arctan \exp x/\lambda$. Time integration is performed according to a predefined accuracy giving sub-picosecond time steps to ensure stability of the numerical scheme. As discussed by Wang *et al.* [58] this is also well below the fastest physical time scales and we are able to capture the details of the exchange interaction. However, sub-picosecond time steps makes the time-integration computationally expensive and puts a limit on the practical grid sizes and time spans that are attainable[2].

When applying a supercritical driving field of 0.5 mT we obtain the magnetization profiles in Figure 3.7. Figure 3.7a shows the longitudinal magnetization m_x and 3.7b shows the transverse magnetization $m_\perp = \sqrt{m_y^2 + m_z^2}$. Consider first the longitudinal magnetization profiles. If the domain wall position is defined as the x-coordinate where $m_x = 0$ we can construct a time-displacement graph for

[2] That sub-picosecond time steps are required to ensure numerical stability is a general problem with explicit integrators. Nonetheless, the major micromagnetics simulation tools such as OOMMF [59] and MuMax [60] manage to produce satisfying results even in three-dimensional spin arrays with explicit integrators by using highly specialized code. Implicit schemes that are stable even at step sizes close to the fastest physical time scales have also been developed [58].

the domain wall and compare our results to the collective coordinate equations, as is done in Figure 3.8. It is obvious that the all-numerical solution is moving faster than the collective coordinate solution. This is in agreement with the results of Wang and Wang [56], who attribute the increased domain wall velocity to spin-wave emission.

Consider next the transverse magnetization profiles. As with the longitudinal magnetization profiles, they demonstrate domain wall displacement, but also the

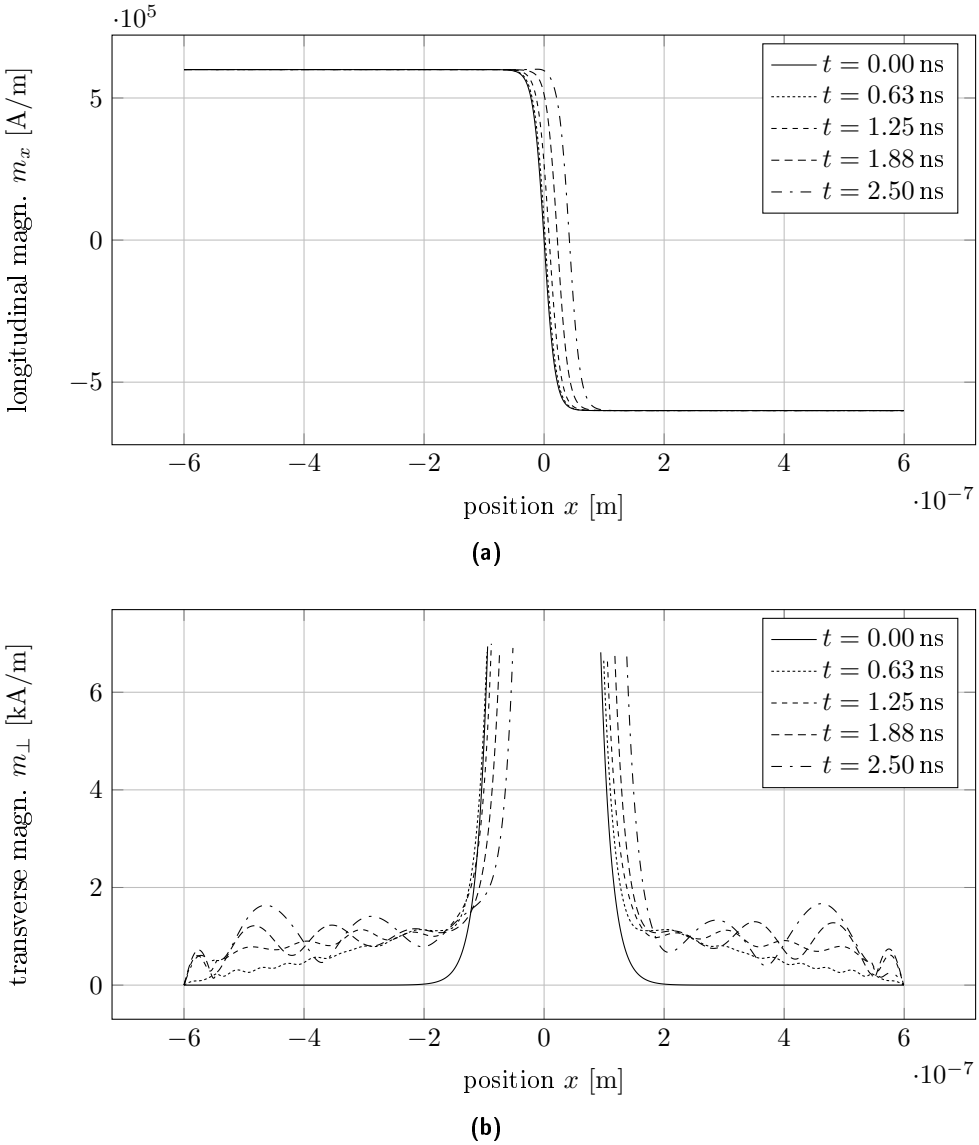

Figure 3.7: Time profiles of (a) longitudinal magnetization m_x and (b) transverse magnetization $m_\perp = \sqrt{m_y^2 + m_z^2}$ under a supercritical driving field of 0.5 mT.

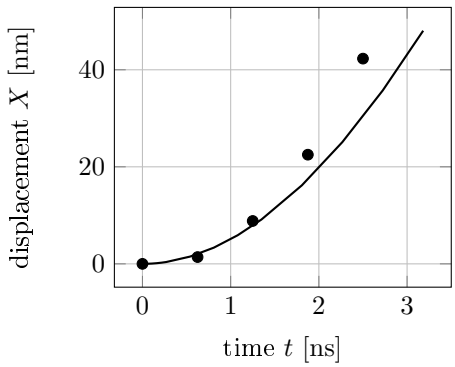

Figure 3.8: Time-displacement data for the all-numerical solution compared to the numerical solution of the collective coordinate equations. Driving field is 0.5 mT (supercritical).

emission of spin waves by the domain wall. Since the spin-wave velocity is (much) larger than the domain wall velocity with permalloy parameters we observe both bow and stern spin-wave emission [52]. However, the difference between bow and stern waves is clearly visible in the profile $m_\perp(t = 2.50\,\mathrm{ns})$. Spin-wave attenuation is easily observable near the ends of the sample, where absorbing boundary conditions are enforced.

3.3.7 Comparison with experiment

A wide range of current induced domain wall behavior has been observed experimentally, but the LLG equation combined with the appropriate wall model appears to be able to qualitatively account for most of the observed phenomena. Refer to Beach *et al.* [20] for an excellent review. However, as pointed out by Beach *et al.* [20] and Thiaville *et al.* [61], the LLG equation is a very general account of torques, and the two spin-transfer torques exhaust the possibility of linearly introducing the gradient in the magnetization along the current direction in the LLG equation. Taken as a phenomenological model, it would thus be at least a little surprising of the LLG equation failed to account for the observed behaviors. To advance our understanding we need to gauge the magnitude of ξ. As is evident from the wide distribution of estimates of ξ, this raises a number of experimental difficulties, although several methods are available [20, 57].

4 Domain wall motion due to magnons

The magnonic spin-transfer torque is the third mechanism by which we can transport ferromagnetic domain walls [19]. Magnons are the quanta of spin oscillations in ordered magnetic structures. However, since the micromagnetic model is a semi-classical model magnons have—strictly speaking—no place in our theory. Instead we should speak of spin-waves. Nonetheless, we will adapt the language of second quantization and speak of magnons as particles although our calculations are semi-classical.

In this chapter we briefly introduce spin-waves and magnons, show how the static domain wall from section 2.3 will move under the influence of spin-waves and discuss other possible mechanisms of magnon-driven domain wall motion.

4.1 Excited states of ferromagnets. Magnons

Magnons or spin-waves are low-lying excitations in ordered magnetic structures. A classical theory for spin-waves can be found in Kittel's *Introduction to solid state physics* [34]. A quantized theory of spin-waves (magnons) is best formulated in second quantization because we are dealing with a many-particle system. Such a theory can be found in Kittel's *Quantum theory of solids* [62]. We repeat here the basic idea behind spin-waves so that we can apply it to a static domain wall and deduce the resulting spin-transfer torque in section 4.2.

Consider the simplest possible model of an ordered magnetic system—a linear chain of N classical spins spaced a apart. The Heisenberg Hamiltonian of this model is given in (2.23),

$$H = -2J \sum_{i=1}^{N} \boldsymbol{S}_i \cdot \boldsymbol{S}_{i+1}.$$

The ground-state of this model is the state where all spins are aligned; then the

energy is $E_0 = 2NJS^2$. We are interested in the low-lying excitations of the chain. By flipping one spin we get a state with energy $E_0 + 8JS^2$. However, we can form an excitation with much lower energy if we let all the spins share the reversal. To do this we consider the equation of motion of a discrete array of spins (2.7),

$$\partial_t \boldsymbol{m}_i = \gamma \boldsymbol{m}_i \times \boldsymbol{H}_i.$$

If the Heisenberg coupling is the only energy functional in the system we can see from the Heisenberg Hamiltonian that

$$\boldsymbol{H}_i = \frac{2J}{\gamma^2}(\boldsymbol{m}_{i-1} + \boldsymbol{m}_{i+1}). \tag{4.1}$$

We write out the equation in Cartesian components and get

$$\partial_t m_i^{(x)} = \frac{2J}{\gamma}\left(m_i^{(y)}\left[m_{i-1}^{(z)} + m_{i+1}^{(z)}\right] - m_i^{(z)}\left[m_{i-1}^{(y)} + m_{i+1}^{(y)}\right]\right)$$

and similarly for the y and the z components. These equations are non-linear because they involve products of the magnetization components. If we let $m^{(z)} = m$ and neglect higher-order terms in $m^{(x)}$ and $m^{(y)}$ we get a set of linear equations,

$$\begin{aligned}
\partial_t m_i^{(x)} &= \frac{2Jm}{\gamma}\left(2m_i^{(y)} - m_{i-1}^{(y)} - m_{i+1}^{(y)}\right), \\
\partial_t m_i^{(y)} &= \frac{2Jm}{\gamma}\left(2m_i^{(x)} - m_{i-1}^{(x)} - m_{i+1}^{(x)}\right), \\
\partial_t m_i^{(z)} &= 0.
\end{aligned}$$

Traveling waves

$$m_p^{(x)} = u \exp i(pka - \omega t), \tag{4.2a}$$

$$m_p^{(y)} = v \exp i(pka - \omega t), \tag{4.2b}$$

solve these equations if the secular equation

$$\hbar\omega = 4JS(1 - \cos ka) \tag{4.3}$$

is fulfilled. Here, we have used $|\gamma| = m/S$ and then changed to dimensionless spins, $S \to \hbar S$, implying $J \to J/\hbar^2$. With this solution $u = iv$.

The dispersion relation (4.3) shows that spin-waves with long wavelengths can have very low excitation energies. In addition, the motivation behind the term spin-wave is evident if we consider the real parts of $m_p^{(x)}$ and $m_p^{(y)}$, namely

$$\begin{aligned}
m_p^{(x)} &= u \cos(pka - \omega t), \\
m_p^{(y)} &= u \sin(pka - \omega t).
\end{aligned}$$

This is circular precession and adjacent spins have a fixed phase relation. If we connect the tips of the magnetization vectors we get a sinusoidal wave pattern, see Figure 4.1.

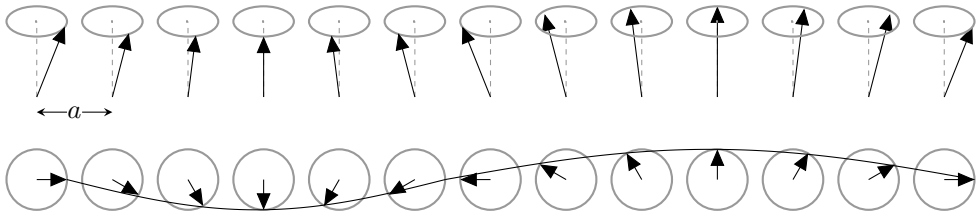

Figure 4.1: A spin-wave on a linear chain of classical spins. The spins are shown in perspective in the upper panel (the vertical axis is the z-axis) and their projection onto the xy-plane is shown in the lower panel. Redrawn after reference [34].

4.2 All-magnonic spin-transfer torque

We are now going to demonstrate that a spin-wave will act with a spin-transfer torque on the static domain wall from section 2.3. Our argument follows that of Yan *et al.* [19].

We are considering a nanowire whose axis coincide with the x-axis. The effective magnetic field is

$$\boldsymbol{H} = \boldsymbol{H}_{\text{ex}} + \boldsymbol{H}_{\text{a}} = \frac{2A}{m^2}\partial_x^2\boldsymbol{m} + \frac{2K}{m^2}m_x\boldsymbol{e}_x.$$

Note that we have neglected the hard axis anisotropy since it did not contribute to the static domain wall profile and since it breaks the cylindrical symmetry of the problem—which will turn out to be important. We assume that the center of the domain wall is positioned at $x = 0$ and that the wall has positive topological charge and chirality, see Figure 3.2.

In order to study magnonic spin-transfer torque we take as an *ansatz* that the magnetization vector is

$$\boldsymbol{m} = m\boldsymbol{e}_r + [m_\vartheta(x)\boldsymbol{e}_\vartheta + m_\varphi(x)\boldsymbol{e}_\varphi]\exp(-i\omega t), \tag{4.4}$$

where ω is the spin-wave angular frequency and the unit vectors $\boldsymbol{e}_r$, $\boldsymbol{e}_\vartheta$ and $\boldsymbol{e}_\varphi$ are defined by the static solution $\boldsymbol{m}_0$, see Figure 4.2. To make sure that the spin-wave is only a perturbation to the static solution we require $\sqrt{m_\vartheta^2 + m_\varphi^2} \ll m$. This is also in keeping with the condition $\partial_t\boldsymbol{m}^2 = 0$ imposed by the LLG equation.

To get the equations for m_ϑ and m_φ we substitute the new parametrization of $\boldsymbol{m}$ back into the LLG equation. Since m_ϑ and m_φ both are small we can neglect higher-order terms such as m_ϑ^2 or $m_\vartheta' m_\varphi$. (The prime denotes a spatial derivative, $m_\vartheta' = \mathrm{d}m_\vartheta/\mathrm{d}x$.) First, we evaluate the exchange term. The spatial derivative is

$$\begin{aligned}\partial_x^2\boldsymbol{m} = m(\partial_x^2\boldsymbol{e}_r) + [&m_\vartheta''\boldsymbol{e}_\vartheta + 2m_\vartheta'(\partial_x\boldsymbol{e}_\vartheta) + m_\vartheta(\partial_x^2\boldsymbol{e}_\vartheta) \\ &+ m_\varphi''\boldsymbol{e}_\varphi + 2m_\varphi'(\partial_x\boldsymbol{e}_\varphi) + m_\varphi(\partial_x^2\boldsymbol{e}_\varphi)]\exp(-i\omega t),\end{aligned}$$

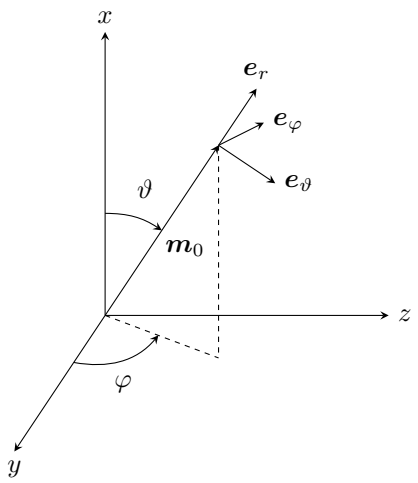

Figure 4.2: The magnetization vector in spherical coordinates. Since ϑ is a function of x the frame spanned by $\boldsymbol{e}_r$, $\boldsymbol{e}_\vartheta$ and $\boldsymbol{e}_\varphi$ will rotate as we move along the x-axis.

where we must also consider the derivatives of the unit vectors[1] since they are functions of x through their dependence on $\vartheta(x)$. Since $\varphi = 0$ the unit vectors in spherical coordinates are given by

$$\boldsymbol{e}_r = +\cos\vartheta \boldsymbol{e}_x + \sin\vartheta \boldsymbol{e}_y, \tag{4.5a}$$

$$\boldsymbol{e}_\vartheta = -\sin\vartheta \boldsymbol{e}_x + \cos\vartheta \boldsymbol{e}_y, \tag{4.5b}$$

$$\boldsymbol{e}_\varphi = \boldsymbol{e}_z. \tag{4.5c}$$

When we evaluate the derivatives of the unit vectors we use the relation (3.21) for the derivative of ϑ that we derived earlier, $\partial_x\vartheta = \sin\vartheta/\lambda$. For the first derivatives we find

$$\partial_x \boldsymbol{e}_r = \frac{\sin\vartheta}{\lambda}(-\sin\vartheta \boldsymbol{e}_x + \cos\vartheta \boldsymbol{e}_y) = \frac{\sin\vartheta}{\lambda}\boldsymbol{e}_\vartheta,$$

and

$$\partial_x \boldsymbol{e}_\vartheta = -\frac{\sin\vartheta}{\lambda}(\cos\vartheta \boldsymbol{e}_x + \sin\vartheta \boldsymbol{e}_y) = -\frac{\sin\vartheta}{\lambda}\boldsymbol{e}_r.$$

[1] One way to solve this problem would be to use (4.5) to reformulate the problem in terms of the Cartesian coordinates and get rid of the unit vector derivatives altogether. However, we choose to keep the spherical coordinates since they capture the symmetry of the problem. When doing the problem in spherical coordinates it turns out that the r-component contributes a trivial equation, while it is the ϑ- and the φ-components who make up the final answer. If we had done the problem in Cartesian coordinates this symmetry would have been much less transparent. The set of three component equations would then have contained only two linearly independent equations and one linear combination of the two.

The second derivative of $\boldsymbol{e}_r$ is

$$\begin{aligned}\partial_x^2\boldsymbol{e}_r =&\partial_x\left(\frac{\sin\vartheta}{\lambda}\boldsymbol{e}_\vartheta\right)=\frac{\sin\vartheta\cos\vartheta}{\lambda^2}\boldsymbol{e}_\vartheta+\frac{\sin\vartheta}{\lambda}(\partial_x\boldsymbol{e}_\vartheta)\\ =&+\frac{\sin\vartheta\cos\vartheta}{\lambda^2}\boldsymbol{e}_\vartheta-\frac{\sin^2\vartheta}{\lambda^2}\boldsymbol{e}_r,\end{aligned}$$

The second derivative of $\boldsymbol{e}_\vartheta$ is

$$\begin{aligned}\partial_x^2\boldsymbol{e}_\vartheta =&\partial_x\left(-\frac{\sin\vartheta}{\lambda}\boldsymbol{e}_r\right)=-\frac{\sin\vartheta\cos\vartheta}{\lambda^2}\boldsymbol{e}_r-\frac{\sin\vartheta}{\lambda}(\partial_x\boldsymbol{e}_r)\\ =&-\frac{\sin\vartheta\cos\vartheta}{\lambda^2}\boldsymbol{e}_r-\frac{\sin^2\vartheta}{\lambda^2}\boldsymbol{e}_\vartheta.\end{aligned}$$

Of course, $\partial_x\boldsymbol{e}_\varphi=0=\partial_x^2\boldsymbol{e}_\varphi$. This gives

$$\begin{aligned}\partial_x^2\boldsymbol{m} =&m\frac{\sin\vartheta\cos\vartheta}{\lambda^2}\boldsymbol{e}_\vartheta-m\frac{\sin^2\vartheta}{\lambda^2}\boldsymbol{e}_r+\left[m_\vartheta''\boldsymbol{e}_\vartheta-2m_\vartheta'\frac{\sin\vartheta}{\lambda}\boldsymbol{e}_r\right.\\ &\left.-m_\vartheta\frac{\sin\vartheta\cos\vartheta}{\lambda^2}\boldsymbol{e}_r-m_\vartheta\frac{\sin^2\vartheta}{\lambda^2}\boldsymbol{e}_\vartheta+m_\varphi''\boldsymbol{e}_\varphi\right]\exp(-i\omega t)\\ =&-\left[m\frac{\sin^2\vartheta}{\lambda^2}+\left(2m_\vartheta'\frac{\sin\vartheta}{\lambda}+m_\vartheta\frac{\sin\vartheta\cos\vartheta}{\lambda^2}\right)\exp(-i\omega t)\right]\boldsymbol{e}_r\\ &+\left[m\frac{\sin\vartheta\cos\vartheta}{\lambda^2}+\left(m_\vartheta''-m_\vartheta\frac{\sin^2\vartheta}{\lambda^2}\right)\exp(-i\omega t)\right]\boldsymbol{e}_\vartheta\\ &+m_\varphi''\exp(-i\omega t)\boldsymbol{e}_\varphi,\end{aligned}$$

which in turn gives

$$\begin{aligned}\gamma\boldsymbol{m}\times\boldsymbol{H}_{\mathrm{ex}} =&-\frac{2\gamma A}{m}\left[m_\varphi\frac{\sin\vartheta\cos\vartheta}{\lambda^2}\boldsymbol{e}_r+\left(m_\varphi''+m_\varphi\frac{\sin^2\vartheta}{\lambda^2}\right)\boldsymbol{e}_\vartheta\right]\exp(-i\omega t)\\ &+\frac{2\gamma A}{m}\left[m\frac{\sin\vartheta\cos\vartheta}{\lambda^2}+m_\vartheta''\exp(-i\omega t)\right]\boldsymbol{e}_\varphi.\end{aligned}$$

Note that the set $\{\boldsymbol{e}_r,\boldsymbol{e}_\vartheta,\boldsymbol{e}_\varphi\}$ is mutually orthonormal so that the cross product can be evaluated using the standard determinant. Second, we evaluate the anisotropy term. In order to evaluate this term we need to express the vector $\boldsymbol{e}_x$ in terms of $\boldsymbol{e}_r$, $\boldsymbol{e}_\vartheta$ and $\boldsymbol{e}_\varphi$. Using the relations (4.5) we find

$$\boldsymbol{e}_x=\cos\vartheta\boldsymbol{e}_r-\sin\vartheta\boldsymbol{e}_\vartheta. \tag{4.6}$$

The component m_x is then given by the dot product,

$$m_x=\boldsymbol{m}\cdot\boldsymbol{e}_x=m\cos\vartheta-m_\vartheta\sin\vartheta\exp(-i\omega t).$$

We also take the cross product between these vectors

$$\begin{aligned}\boldsymbol{m}\times\boldsymbol{e}_x =&m_\varphi\sin\vartheta\exp(-i\omega t)\boldsymbol{e}_r+m_\varphi\cos\vartheta\exp(-i\omega t)\boldsymbol{e}_\vartheta\\ &-[m\sin\vartheta+m_\vartheta\cos\vartheta\exp(-i\omega t)]\boldsymbol{e}_\varphi.\end{aligned}$$

Using the dot product, the cross product and the prefactor we are ready to assemble the anisotropy term,

$$\begin{aligned}\gamma \boldsymbol{m} \times \boldsymbol{H}_{\mathrm{a}} = \frac{2\gamma K}{m}\Big[& - m_\varphi \sin\vartheta\cos\vartheta \exp(-i\omega t)\boldsymbol{e}_r + m_\varphi \cos^2\vartheta \exp(-i\omega t)\boldsymbol{e}_\vartheta \\ & - [m \sin\vartheta\cos\vartheta - m_\vartheta \sin^2\vartheta \exp(-i\omega t) \\ & + m_\vartheta \cos^2\vartheta \exp(-i\omega t)]\boldsymbol{e}_\varphi\Big].\end{aligned}$$

Third, we evaluate the damping term. The time derivative is

$$\partial_t \boldsymbol{m} = -i\omega[m_\vartheta \boldsymbol{e}_\vartheta + m_\varphi \boldsymbol{e}_\varphi]\exp(-i\omega t),$$

giving

$$\frac{\alpha}{m}\boldsymbol{m} \times \partial_t \boldsymbol{m} = i\omega\alpha[m_\varphi \boldsymbol{e}_\vartheta - m_\vartheta \boldsymbol{e}_\varphi]\exp(-i\omega t).$$

By substituting these terms into the LLG equation we get the following three component equations. The r-component gives

$$0 = -\frac{2\gamma A}{m\lambda^2} m_\varphi \sin\vartheta\cos\vartheta + \frac{2\gamma K}{m} m_\varphi \sin\vartheta\cos\vartheta.$$

By using the definition $\lambda^2 = A/K$ we see that the two terms on the right-hand side are identical, so that the equation is in fact trivial. Using the same identity, the ϑ-component gives

$$-i\omega m_\vartheta = -\frac{2\gamma A}{m} m_\varphi'' + \frac{2\gamma K}{m} m_\varphi(\cos^2\vartheta - \sin^2\vartheta) + i\omega\alpha m_\varphi,$$

and the φ-component gives

$$-i\omega m_\varphi = +\frac{2\gamma A}{m} m_\vartheta'' - \frac{2\gamma K}{m} m_\vartheta(\cos^2\vartheta - \sin^2\vartheta) - i\omega\alpha m_\vartheta$$

It is these two equations that contribute to the final result. Using a trigonometric identity we get the following pair of coupled differential equations for m_ϑ and m_φ,

$$-i\omega m_\vartheta = -\frac{2\gamma A}{m} m_\varphi'' - \frac{2\gamma K}{m} m_\varphi(2\sin^2\vartheta - 1) + i\omega\alpha m_\varphi, \tag{4.7}$$

$$-i\omega m_\varphi = +\frac{2\gamma A}{m} m_\vartheta'' + \frac{2\gamma K}{m} m_\vartheta(2\sin^2\vartheta - 1) - i\omega\alpha m_\vartheta. \tag{4.8}$$

These equations can be recast into a single differential equation if we define

$$\psi(x) = m_\vartheta(x) - i m_\varphi(x); \tag{4.9}$$

just multiply the first equation by i, add the two and get

$$\omega\psi = \frac{2\gamma A}{m}\frac{\mathrm{d}^2}{\mathrm{d}x^2}\psi + \frac{2\gamma K}{m}(2\sin^2\vartheta - 1)\psi - i\omega\alpha\psi.$$

Now use the definition of the domain wall width, $\lambda^2 = A/K$, and the relation (3.24) for the sine of ϑ that we derived earlier, $\sin\vartheta = \operatorname{sech}(x/\lambda)$, giving

$$\left[\omega(1+i\alpha) + \frac{2\gamma K}{m}\right]\psi = \frac{2\gamma K}{m}\lambda^2\frac{\mathrm{d}^2}{\mathrm{d}x^2}\psi + \frac{4\gamma K}{m}\operatorname{sech}^2(x/\lambda).$$

Define the dimensionless length $\zeta = x/\lambda$ and divide by $-2\gamma K/m$ to get

$$q^2\psi(\zeta) = \left[-\frac{\mathrm{d}^2}{\mathrm{d}\zeta^2} - 2\operatorname{sech}^2\zeta\right]\psi(\zeta) \tag{4.10}$$

where we have defined $q^2 = -m\omega(1+i\alpha)/2\gamma K - 1$. Mind again that our convention is $\gamma < 0$ and $K > 0$. This equation is well-known and has been solved.

Equation (4.10) is in the form of a dimensionless Schrödinger equation. It can be solved either by a direct approach [63, 64] or by constructing ladder operators [64, 65]. It has two solutions: a bound state

$$\psi(\zeta) = \tfrac{1}{2}\operatorname{sech}\zeta \tag{4.11}$$

for $q = -i$ (which implies $\omega = 0$) and a traveling wave

$$\psi(\zeta) = -\rho\left(\frac{\tanh\zeta - iq}{1+iq}\right)\exp(iq\zeta) \tag{4.12}$$

for $q > 0$. The asymptotic behavior of the hyperbolic tangent, $\lim_{\zeta\to\infty}\tanh\zeta = 1$, and the fact that the hyperbolic tangent is an odd function of ζ makes the asymptotic behavior of the second solution especially simple,

$$\lim_{\zeta\to-\infty}\psi = \rho\exp(iq\zeta)$$

and

$$\lim_{\zeta\to+\infty}\psi = -\rho\left(\frac{1-iq}{1+iq}\right)\exp(iq\zeta).$$

This means that in the absence of damping (that is, $\alpha = 0$) any non-zero spin-wave angular frequency will produce a spin-wave that travels right through the domain wall except for a change in phase. This interesting behavior makes the potential $\operatorname{sech}^2\zeta$ a reflectionless potential. Its most basic properties are explored in Problem 2.51 in reference [29]. A more thorough treatment can be found in reference [66]. In the presence of damping the wave vector is complex. The imaginary part will then contribute an exponential decay—so the presence of damping in the material simply gives damped spin-waves as a result.

A change in phase upon the interaction between a spin-wave and a domain wall means that spin is transferred from the spin-wave to the domain wall, so we have a spin-transfer torque. This is easily seen from the asymptotic from of the traveling waves above: in the limit of long wavelength excitations the wave vector

is small, so the change in phase goes to π. Such a phase reversal of a spin-wave corresponds to flipping the spin of a magnon. A corresponding change in spin must take place in the domain wall—so spin is transferred from the magnon to the wall and there is a spin torque. If we visualize the phase change as it takes place in our head-to-head wall this becomes even clearer. Figure 4.3 shows the head-to-head wall. As we go from one domain to the next the direction of the precessing spins averaged over one period flips 180°. The domain wall must travel in the opposite direction of the spin-waves.

The phase shift we have derived is exact in the limit of weak spin-wave excitations, but our strategy for finding the phase shift required that the domain wall profile could be solved analytically. Bayer *et al.* [67] have developed a WKB approximation to estimate the phase shift when simple analytical solutions are not available, for instance in some cases of domain wall pinning.

4.2.1 The magnonic spin-transfer torque in terms of the magnetization current. Domain wall velocity

The magnonic spin-transfer torque can also be understood in terms of the magnetization current. The presence of damping obscures this picture, so in the following we are going to set $\alpha = 0$. The LLG equation of our system is then simply

$$\partial_t \boldsymbol{m} = \frac{2\gamma A}{m^2} \boldsymbol{m} \times \partial_x^2 \boldsymbol{m} + \frac{2\gamma K}{m^2} m_x (\boldsymbol{m} \times \boldsymbol{e}_x).$$

Since

$$\partial_x (\boldsymbol{m} \times \partial_x \boldsymbol{m}) = \partial_x \boldsymbol{m} \times \partial_x \boldsymbol{m} + \boldsymbol{m} \times \partial_x^2 \boldsymbol{m} = \boldsymbol{m} \times \partial_x^2 \boldsymbol{m}$$

we can write

$$\partial_t \boldsymbol{m} = \frac{2\gamma K}{m^2} m_x (\boldsymbol{m} \times \boldsymbol{e}_x) + \partial_x \boldsymbol{J} \tag{4.13}$$

where

$$\boldsymbol{J} = \frac{2\gamma A}{m^2} \boldsymbol{m} \times \partial_x \boldsymbol{m} \tag{4.14}$$

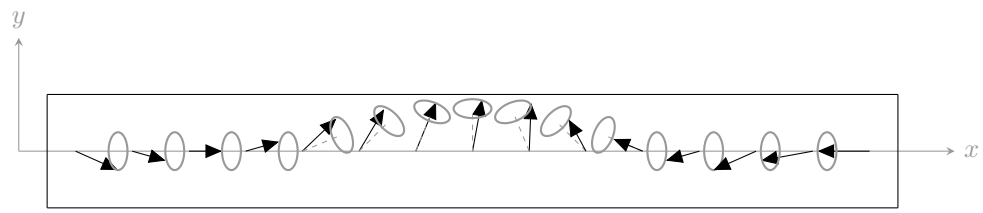

Figure 4.3: Spin-wave in a head-to-head Néel wall.

is named the magnetization current density [19, 68]. This name is justified when we observe that the x-component of (4.13) has no contribution from the anisotropy term and thus gives the continuity equation

$$\partial_t m_x + \partial_x J_x = 0. \tag{4.15}$$

However, equation (4.14) does not provide a very transparent or useful expression for the magnetization current. Thus, we write out equation (4.14) using equation (4.4) to find a better form. Using our expressions for the first derivatives of the spherical unit vectors we get

$$\begin{aligned}\partial_x \boldsymbol{m} =& m(\partial_x \boldsymbol{e}_r) + [m'_\vartheta \boldsymbol{e}_\vartheta + m_\vartheta(\partial_x \boldsymbol{e}_\vartheta) + m'_\varphi \boldsymbol{e}_\varphi]\exp(-i\omega t)\\ =& m\frac{\sin\vartheta}{\lambda}\boldsymbol{e}_\vartheta + \left[m'_\vartheta \boldsymbol{e}_\vartheta - m_\vartheta \frac{\sin\vartheta}{\lambda}\boldsymbol{e}_r + m'_\varphi \boldsymbol{e}_\varphi\right]\exp(-i\omega t)\\ =& -m_\vartheta \frac{\sin\vartheta}{\lambda}\exp(-i\omega t)\boldsymbol{e}_r + \left[m\frac{\sin\vartheta}{\lambda} + m'_\vartheta \exp(-i\omega t)\right]\boldsymbol{e}_\vartheta\\ &+ m'_\varphi \exp(-i\omega t)\boldsymbol{e}_\varphi.\end{aligned}$$

By taking the cross product with $\boldsymbol{m}$ and the dot product with $\boldsymbol{e}_x$ (4.6) we arrive at

$$\begin{aligned}J_x =& \frac{2\gamma A}{m^2}\left[m_\vartheta m'_\varphi \exp(-i\omega t) - m\frac{\sin\vartheta}{\lambda}m_\varphi - m_\varphi m'_\vartheta \exp(-i\omega t)\right]\cos\vartheta\\ &\times \exp(-i\omega t) + \frac{2\gamma A}{m^2}\left[m m'_\varphi + m_\vartheta m_\varphi \frac{\sin\vartheta}{\lambda}\exp(-i\omega t)\right]\sin\vartheta\exp(-i\omega t).\end{aligned}$$

Being interested in the magnitude of the magnetization current we observe that the time-dependent exponentials have unity modulus and can be dropped. In addition $\sin\vartheta \to 0$ and $\cos\vartheta \to \pm 1$ in the domains so this expression simplifies to

$$J_x = \pm\frac{2\gamma A}{m^2}(m_\vartheta m'_\varphi - m_\varphi m'_\vartheta).$$

The crucial observation is that this same expression can be obtained from the form

$$J_x = \frac{\gamma A}{i\lambda m^2}(\psi\partial_\zeta\psi^* - \psi^*\partial_\zeta\psi)\cos\vartheta \tag{4.16}$$

using the definition (4.9) and the limit $\cos\vartheta \to \pm 1$:

$$\begin{aligned}J_x =& \pm\frac{\gamma A}{im^2}(m_\vartheta - im_\varphi)(m'_\vartheta + im'_\varphi) \mp \frac{\gamma A}{im^2}(m_\vartheta + im_\varphi)(m'_\vartheta - im'_\varphi)\\ =& \pm\frac{2\gamma A}{m^2}(m_\vartheta m'_\varphi - m_\varphi m'_\vartheta).\end{aligned}$$

The expression (4.16) is a very interesting form. It is in fact the same form as that of the probability current density known from introductory quantum mechanics

[29], only that ψ expresses now magnetization density and not the probability to find a particle.

Next, we use equation (4.16) to calculate the magnetization current in the two domains with the help of (4.12). Since

$$\partial_\zeta \psi = iq\psi - \frac{\rho}{1-iq}\frac{\exp(-iq\zeta)}{\cosh^2\zeta}$$

we get

$$\begin{aligned} J_x &= \mp\frac{\gamma A}{i\lambda m^2}\left[2iq\psi^*\psi - \frac{\rho^2(\tanh\zeta - iq)}{(1+q^2)\cosh^2\zeta} + \frac{\rho^2(\tanh\zeta + iq)}{(1+q^2)\cosh^2\zeta}\right] \\ &= \mp\frac{2\gamma A q}{\lambda m^2}\left[\psi^*\psi - \frac{\rho^2\sin^2\vartheta}{1+q^2}\right], \end{aligned}$$

where we used equation (3.24). Since the wave vector k is given by $k = q/\lambda$ we find

$$J_x = -\frac{2\gamma A\rho^2 k}{m^2}$$

in the limit $\zeta \to -\infty$ and

$$J_x = +\frac{2\gamma A\rho^2 k}{m^2}$$

in the limit $\zeta \to +\infty$. The magnetization current changes sign after passing through the domain wall and will, as a result, exert a spin-transfer torque on the wall. Since $J_x = mv_x$ the domain wall must travel to the left with a velocity

$$\boldsymbol{v} = -\frac{2\gamma A\rho^2 k}{m^3}\boldsymbol{e}_x = -\frac{\rho^2 v_\mathrm{g}}{2m^2}\boldsymbol{e}_x, \tag{4.17}$$

to absorb this torque. Here, v_g is the group velocity of the spin-waves,

$$v_\mathrm{g} = \frac{\mathrm{d}\omega}{\mathrm{d}k} = \frac{4\gamma K\lambda^2 k}{m} = \frac{4\gamma A k}{m},$$

since $\omega = -(2\gamma K/m)(\lambda^2 k^2 + 1)$.

4.2.2 Numerical studies of magnon-driven domain walls

Several numerical studies of magnon-driven domain walls have been conducted [19, 69–75]. A number of these studies support a domain wall velocity depending on the square of the spin-wave amplitude [19, 74, 75]. A quadratic dispersion relation has also been found numerically [74]. Remarkably, these results are robust even in the presence of a perpendicular hard axis magnetic anisotropy, even though such a term breaks the cylindrical symmetry of the problem.

In addition to these findings, which support the existence of a magnonic spin-transfer torque, a number of other results show that there is more to magnon-driven domain wall transport than the spin-transfer torque. In particular, domain wall motion by spin transfer is only consistent with domain wall propagation opposite to the spin-wave propagation direction. Domain wall motion parallel to the spin-wave propagation direction has repeatedly been observed [69–75]. Moreover, numerical findings show a strong dependence of the domain wall velocity on the spin-wave frequency [69–75]. It has been proposed that these issues can be resolved by introducing a second mechanism of magnon-driven domain wall motion: linear momentum transfer [72, 73, 76, 77]. Linear momentum transfer is consistent with domain wall motion parallel to the spin-wave propagation direction, and the linear momentum mechanism has shown a strong dependence on the resonance conditions of the interaction of the spin-wave with the domain wall, possibly explaining the strong dependence of domain wall velocity on spin-wave frequency.

Since spin-wave excitations of the magnetic lattice does not depend on excitation of a charge current, devices based on all-magnonic domain wall transport can be made from ferromagnetic insulators [19]. This is an opportunity to altogether avoid Joule heating in the active part of the device, which would be an important improvement of the spintronic devices that have already been proposed. In addition, the intriguing possibility of performing logic operations based on the phase change induced in a spin-wave by interacting with a domain wall has also been proposed [78].

5 Conclusion and outlook

We have reviewed the Landau-Lifshitz-Gilbert equation and solved it in the static case and for field-, current- and magnon-driven motion. Our treatment of field- and current-driven motion included a comprehensive approach to domain wall expansion and contraction inspired by references [5, 11, 52, 61, 79]. Unlike Shibata *et al.* [5] we included a variable domain wall width in the collective coordinate approach. Unlike Thiaville *et al.* [61, 79] we derive our expressions directly from the LLG equation, not from the Lagrangian. Unlike Li and Zhang [11] we claim that our treatment based on Walker's *ansatz* is valid in the supercritical regime, thus explaining breathing. This phenomenon was observed numerically by Wang *et al.* [52] and correctly attributed to an expression for a variable domain width similar to the one derived here, which was first derived by Schryer and Walker [18].

Our treatment of the magnon-driven motion was a reproduction of the results obtained by Yan *et al.* [19], but included Gilbert damping. We thus demonstrated analytically that this gives an exponential damping of the spin-waves, a fact that was also exploited by implementing of non-reflection boundary conditions in the all-numerical solution of field-driven motion.

In field and current induced motion Walker breakdown occurs when the driving forces reach a critical value. We have seen the differences in domain wall behavior in the sub- and supercritical regimes, as well as the differences in microscopic mechanisms leading to wall translation. To avoid loss of information by domain wall deformation, it is important to operate devices based on field or spin-transfer torques below the threshold for Walker breakdown. To the best of our knowledge, the mechanism and conditions for Walker breakdown in magnon propagated domain wall motion has not been studied. All-magnonic wall motion offers an intriguing possibility to avoid Joule heating, and the limits on domain wall velocity imposed by wall deformation thus deserves attention in order to bring the theory of magnon induced motion closer to the level of the field and current induced motion.

Other topics for further studies includes the effect on magnon-driven domain

wall motion of more advanced interactions such as Dzyaloshinskii-Moriya interactions and spin-orbit coupling. Such studies are analogous to the studies of these effects on field- and current driven motion [80, 81], which have only recently been attempted, and they are a natural extension of the theory of magnon induced motion once the condition for Walker breakdown has been established.

A Solving ODEs numerically using Matlab

Ordinary differential equations (ODEs) are differential equations describing functions y that only depend on one variable x. Introductory texts that treat ODEs include Boas [31] and Kreyszig [82]. ODEs can be of any order, *i.e.* there is no limit on the order of the highest derivative. An example of a second order ODE is

$$\frac{\mathrm{d}^2 y}{\mathrm{d}x^2} + q(x)\frac{\mathrm{d}y}{\mathrm{d}x} = r(x).$$

However, such an equation can always be rewritten as a set of first order equations:

$$y' = z,$$
$$z' = r - qz,$$

where in this case z is a new variable, defined to be the derivative y'. So an nth order equation can be written as n first order equations. Ordinarily, the new variables will—as in the case above—be chosen as the derivatives of the function of interest. However, there is no reason why other functions (or constants) cannot be included in the definitions if this is convenient.

Because higher order equations can be reduced to first order equations interest in solving ODEs is mainly focused at solving first order ODEs and systems of first order ODEs. So the general case we look at is a set of n equations on the form

$$y_i' = f_i(x, y_1, \ldots, y_n) \tag{A.1}$$

for $i = 1, \ldots, n$, where the functions f_i are known. Such equations divide into two classes of numerical problems depending on the boundary conditions that are available [83]:

- Initial value problems. If all the necessary boundary conditions (one per equation in the first order system) are given at a single point x_0 then the problem and its solution is completely specified at that point. Our task is then to propagate that solution through the interval of interest.

- Boundary value problems. If the necessary boundary conditions are specified at more than one point—typically at the two interval endpoints x_s and x_f—then the problem and its solution is not completely specified anywhere. Our task is then to guess a solution and relax it iteratively to the solution.

We will only consider initial value problems here. The basic idea is to propagate the known solution through the interval of interest using the scheme

$$y_{k+1} = y_k + h \cdot f_k. \tag{A.2}$$

A direct implementation of this iteration scheme is known as Euler's method. In practice we use more sophisticated schemes. For example, we might stop at $x_k + \frac{1}{2}h$—halfway through the full step h—and correct our value f_k. This can be done in various ways. We can simply use the average of f_k and the preliminary f^*_{k+1},

$$y_{k+1} = y_k + \tfrac{1}{2}h[f(x_k, y_k) + f(x_{k+1}, y^*_{k+1})] \tag{A.3}$$

(improved Euler method), or we can make a more sophisticated correction,

$$\begin{aligned} c_1 &= f(x_k, y_k), \\ c_2 &= f(x_k + \tfrac{1}{2}h, y_k + \tfrac{1}{2}hc_1), \\ c_3 &= f(x_k + \tfrac{1}{2}h, y_k + \tfrac{1}{2}hc_2), \\ c_4 &= f(x_k + h, y_k + hc_3), \\ y_{k+1} &= y_k + \tfrac{1}{6}h(c_1 + 2c_2 + 2c_3 + c_4) \end{aligned} \tag{A.4}$$

(fourth order Runge-Kutta method). The accuracy of the solution depends on the step length h.

The methods we have considered so far are one-step methods. It is also possible to construct multistep methods, *i.e.* methods that use information from two or more previous steps to compute the next step. A minor challenge related to multistep methods is that they are not self-starting; since we originally only know one point we need to use a one-step method to find the next few steps in order to get the multistep calculation started. Once this has been done, multistep methods are in principle just as simple as one-step methods. The most widely known multistep methods are the Adams-Bashford methods and the Adams-Moulton methods.

Before we start looking at the available MATLAB routines for solving ODEs, we need to introduce the term *stiffness*. Stiffness is not very often formally defined, but the general disease is that above a certain step length time propagation does not seem to give sensible results. It is easy to understand the reason for this if we look closer at the Euler scheme (A.2). Since $y' = f$ the Euler scheme is essentially a truncation of a Taylor series at first order. It follows that the leading error term will be of second order. What happens when we let h increase is that the error grows as h^2, while the solution grows as h. This is alright if the difference is offset by y' growing faster than y'' (as would be the case for a polynomial). But if that is

not the case, our solution is in trouble because our numerical scheme is no longer stable. Stiff equations are equations where the error term grows faster than the solution, restricting us to small step sizes. Typically, this is the case if the solution involves two functions that are characterized by very different length scales. (This could be, say, an exponential and a polynomial.) Schemes that are stable for stiff equations are typically implicit schemes,

$$y_{k+1} = y_k + h \cdot f_{k+1}. \tag{A.5}$$

(backward Euler method). Examples of more sophisticated implicit schemes are the Rosenbrock methods (which are one-step methods based on Runge-Kutta methods) and Gear's backward differentiation methods (which are multistep methods based on numerical differentiation formulas).

MATLAB provides several routines for solving ODEs [84]. Some are meant to give rough and ready solutions, others provide higher precision. All built-in routines that solve explicit ODEs in MATLAB are addressed in the same way. A common feature is that systems of ODEs are handled just as easily as single equations—just change scalars to vectors.

- `ode45`. Uses simultaneously fourth and fifth order Runge-Kutta formulas to make error estimates and adjust the step size (adaptive step size control). MATLAB recommends that `ode45` is used as a first solver for non-stiff problems.

- `ode23`. Uses simultaneously second and third order Runge-Kutta formulas for adaptive step size control. `ode23` is less expensive computationally than `ode45`, but of lower order. It may be more efficient than `ode45` presented with mild stiffness, especially at crude tolerances.

- `ode113`. Uses a variable-order Adams-Bashford-Moulton solver. `ode113` is intended for non-stiff problems with stringent error tolerances or for solving computationally intensive problems.

There are also a number of solvers intended for stiff problems. Among them, `ode15s` is the first solver, but `ode23s` may be more efficient—especially at crude tolerances. Other solvers for stiff problems are `ode23t` and `ode23tb`. In addition there is `ode15i` for fully implicit equations.

B Solving PDEs numerically using Matlab

Partial differential equations (PDEs) are differential equations describing functions u that depend on two or more variables $x, y, \ldots$ Introductory texts that treat PDEs include Boas [31] and Kreyszig [82]. Naturally, the theory of PDEs is a vast subject and the present treatment will be limited to problems involving only two independent variables, x and y, and to quasilinear second order equations, that is, second order equations that are linear in the highest derivatives. Such equations can be written on the form

$$a(x,y)u_{xx} + 2b(x,y)u_{xy} + c(x,y)u_{yy} = f(x,y,u,u_x,u_y), \tag{B.1}$$

where we have written $\partial_x u = u_x$. Based on the value of the discriminant $ac - b^2$ they can be classified as either hyperbolic, parabolic or elliptic, see Table B.1. Note that since a, b and c can be functions of the independent variables, it is possible to have equations of mixed type—equations that are of different type in different regions of the xy-plane.

The division into hyperbolic, parabolic or elliptic equations is more important in analytical approaches to these equations than in numerical schemes [83]. Both hyperbolic and parabolic equations give rise to initial value problems (or Cauchy problems) while elliptic equations give rise to boundary value problems. As explained in Appendix A solving an initial value problem or a boundary value problem are numerically quite different tasks. In the case of a boundary value

Table B.1: Classification of partial differential equations.

condition	type	example
$ac - b^2 < 0$	hyperbolic	wave equation, $u_{tt} = v^2 u_{xx}$
$ac - b^2 = 0$	parabolic	diffusion equation, $u_t = D u_{xx}$
$ac - b^2 > 0$	elliptic	Poisson equation, $u_{xx} + u_{yy} = \rho(x,y)$

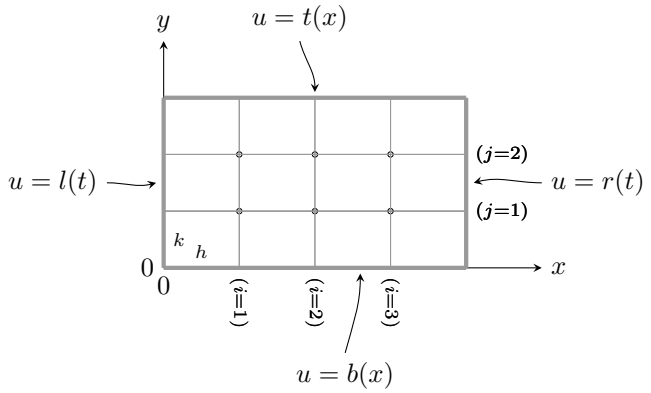

Figure B.1: Solving partial differential equations by discretization. Boundary value problems must be solved by relaxation.

problem we must find a scheme that relaxes to a self-consistent solution inside the boundary as in Figure B.1, but in the case of an initial value problem we can seek ways to propagate the solution in time as in Figure B.2.

Partial differential equations can be solved numerically by replacing the exact equation by a set of difference equations that can be obtained from truncated Taylor expansions. Use

$$\begin{aligned}
u(x+h,y) &= u(x,y) + hu_x(x,y) + \tfrac{1}{2}h^2u_{xx}(x,y) + \dots \\
u(x-h,y) &= u(x,y) - hu_x(x,y) + \tfrac{1}{2}h^2u_{xx}(x,y) - \dots \\
u(x,y+k) &= u(x,y) + ku_y(x,y) + \tfrac{1}{2}h^2u_{yy}(x,y) + \dots \\
u(x,y-k) &= u(x,y) - ku_y(x,y) + \tfrac{1}{2}h^2u_{yy}(x,y) - \dots
\end{aligned}$$

to solve for

$$u_x(x,y) \approx \frac{1}{2h}[u(x+h,y) - u(x-h,y)], \tag{B.2a}$$

$$u_y(x,y) \approx \frac{1}{2k}[u(x,y+k) - u(x,y-k)], \tag{B.2b}$$

$$u_{xx}(x,y) \approx \frac{1}{h^2}[u(x+h,y) - 2u(x,y) + u(x-h,y)], \tag{B.2c}$$

$$u_{yy}(x,y) \approx \frac{1}{k^2}[u(x,y+k) - 2u(x,y) + u(x,y-k)], \tag{B.2d}$$

which are the difference quotients. Using the parabolic diffusion equation as an example,

$$u_t = u_{xx},$$

equating the difference quotients gives the difference equation

$$\frac{1}{k}(u_{i,j+1} - u_{i,j}) = \frac{1}{h^2}(u_{i+1,j} - 2u_{i,j} + u_{i-1,j}), \tag{B.3}$$

where we have used a forward difference quotient on the left-hand side since we have no information for negative t values. With this equation in hand we can solve for u at $t = (j+1)k$ using the function values at $t = jk$, thus propagating the solution in time, see Figure B.2. The Courant condition [82, 83] for the convergence of this method is $r = k/h^2 \leq \frac{1}{2}$.

Parabolic and elliptic initial-boundary value problems can be solved in one space variable and time in MATLAB using the predefined routine `pdepe` [85]. This solver uses space discretization and performs the time integration using `ode15s`, which is capable of solving the differential-algebraic equations that arise when there are elliptic equations in the original PDE system, and can handle the resulting sparse matrices in a memory-efficient way. `ode15s` uses variable-order numerical differentiation formulas (NDFs), or, optionally, backward differentiation formulas (Gear's method). As with ODEs, systems of PDEs are solved by exchanging vectors for scalars.

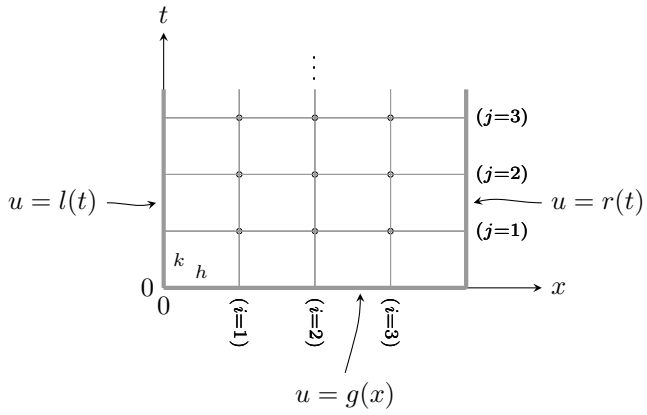

Figure B.2: Solving partial differential equations by discretization. Initial value problems can be solved by time propagation.

Bibliography

As far as possible, original research literature is cited. A number of review articles are also included for easier access to the main lines of development. For older articles, reprints (if available) are included as well as the original reference.

1. M. Lakshmanan, Philosophical Transactions of the Royal Society A **369**, 1280 (2011), review.

2. J. A. Katine and E. F. Fullerton, Journal of Magnetism and Magnetic Materials **320**, 1217 (2008), review.

3. A. Brataas, A. D. Kent, and H. Ohno, Nature Materials **11**, 372 (2012), review.

4. D. C. Ralph and M. D. Stiles, Journal of Magnetism and Magnetic Materials **320**, 1190 (2008), review.

5. J. Shibata, G. Tatara, and H. Kohno, Journal of Physics D: Applied Physics **44**, 384004 (2011), review.

6. Everspin Technologies, Everspin Technologies press release, "Everspin debuts first spin-torque MRAM for high performance storage systems," `http://www.everspin.com/` (2012), [Online; accessed November 22, 2014].

7. S. S. P. Parkin, M. Hayashi, and L. Thomas, Science **320**, 190 (2008).

8. M. Hayashi, L. Thomas, R. Moriya, C. Rettner, and S. S. P. Parkin, Science **320**, 209 (2008).

9. S. Matsunaga, J. Hayakawa, S. Ikeda, K. Miura, H. Hasegawa, T. Endoh, H. Ohno, and T. Hanyu, Applied Physics Express **1**, 091301 (2008).

10. D. A. Allwood, G. Xiong, C. C. Faulkner, D. Atkinson, D. Petit, and R. P. Cowburn, Science **309**, 1688 (2008).

11. Z. Li and S. Zhang, Physical Review B **70**, 024417 (2004).

12. A. Yamaguchi, T. Ono, S. Nasu, K. Miyake, K. Mibu, and T. Shinjo, Physical Review Letters **92**, 077205 (2004).

13. S. Zhang and Z. Li, Physical Review Letters **93**, 127204 (2004).

14. G. Tatara and H. Kohno, Physical Review Letters **92**, 086601 (2004).

15. M. D. Stiles, W. M. Saslow, M. J. Donahue, and A. Zangwill, Physical Review B **75**, 214423 (2007).

16. P. J. Metaxas, J. Sampaio, A. Chanthbouala, R. Matsumoto, A. Anane, A. Fert, K. A. Zvezdin, K. Yakushiji, H. Kubota, A. Fukushima, S. Yuasa, K. Nishimura, Y. Nagamine, H. Maehara, K. Tsunekawa, V. Cros, and J. Grollier, Scientific Reports **3**, 1829 (2013).

17. A. Yamaguchi, S. Nasu, H. Tanigawa, T. Ono, K. Miyake, K. Mibu, and T. Shinjo, Applied Physics Letters **86**, 012511 (2005).

18. N. L. Schryer and L. R. Walker, Journal of Applied Physics **45**, 5406 (1974).

19. P. Yan, X. S. Wang, and X. R. Wang, Physical Review Letters **107**, 177207 (2011).

20. G. S. D. Beach, M. Tsoi, and J. L. Erskine, Journal of Magnetism and Magnetic Materials **320**, 1272 (2008), review.

21. A. Aharoni, Physica B **306**, 1 (2001), review.

22. T. Heinzel, *Mesoscopic electronics in solid state nanostructures*, 2nd ed. (Wiley-VCH Verlag, 2007).

23. S. Datta, *Electronic transport in mesoscopic systems* (Cambridge University Press, 1997).

24. C. Herring and C. Kittel, Physical Review **81**, 869 (1951).

25. L. D. Landau and E. M. Lifshitz, Physikalische Zeitschrift Sowjetunion **8**, 153 (1935); L. D. Landau, in *Collected papers of L. D. Landau*, edited by D. ter Haar (Pergamon Press and Gordon and Breach Science Publishers, 1965) Chap. 18.

26. T. L. Gilbert and J. M. Kelly, in *Conference of Magnetism and Magnetic Materials* (AIEE, Pittsburgh, PA, USA, 1955) pp. 253–263.

27. T. L. Gilbert, Physical Review **100**, 1243 (1955).

28. T. L. Gilbert, IEEE Transactions on Magnetics **40**, 3443 (2004), review.

29. D. J. Griffiths, *Introduction to quantum mechanics*, 2nd ed. (Pearson, 2013).

30. J. J. Sakurai and J. Napolitano, *Modern quantum mechanics*, 2nd ed. (Addison-Wesley, 2011).

31. M. L. Boas, *Mathematical methods in the physical sciences*, 3rd ed. (John Wiley & Sons, 2006).

32. H. Goldstein, C. P. Poole, and J. L. Safko, *Classical mechanics*, 3rd ed. (Addison-Wesley, 2001).

33. R. P. Feynman, R. B. Leighton, and M. Sands, *The Feynman lectures on physics*, new millenium ed. (Basic Books, 2010).

34. C. Kittel, *Introduction to solid state physics*, 5th ed. (John Wiley & Sons, 1976).

35. E. C. Stoner and E. P. Wohlfarth, Philosophical Transactions of the Royal Society of London A **240**, 599 (1948); IEEE Transactions on Magnetics **27**, 3475 (1991).

36. R. C. O'Handley, *Modern magnetic materials. Principles and applications* (John Wiley & Sons, 2000).

37. A. Auerbach, *Interacting electrons and quantum magnetism* (Springer-Verlag, 1994).

38. M. Mulazzi, A. Chainani, Y. Takata, Y. Tanaka, Y. Nishino, K. Tamasaku, T. Ishikawa, T. Takeuchi, Y. Ishida, and Y. Senba, Physical Review B **77**, 224425 (2008).

39. E. Kreyszig, *Introductory functional analysis* (John Wiley & Sons, 1978).

40. C. Kittel, Reviews of Modern Physics **21**, 541 (1949), review.

41. G. Tatara, H. Kohno, and J. Shibata, Physics Reports **468**, 213 (2008), review.

42. L. Berger, Journal of Applied Physics **49**, 2156 (1978).

43. L. Berger, Journal of Applied Physics **50**, 2137 (1979).

44. M. N. Baibich, J. M. Broto, A. Fert, F. N. van Dau, F. Petroff, P. Etienne, G. Creuzet, A. Friederich, and J. Chazelas, Physical Review Letters **61**, 2472 (1988).

45. G. Binasch, P. Grünberg, and F. Saurenbach, Physical Review B **39**, 4828 (1989).

46. J. C. Slonczewski, Journal of Magnetism and Magnetic Materials **159**, L1 (1996).

47. L. Berger, Physical Review B **54**, 9353 (1996).

48. H. Kohno and J. Shibata, Journal of the Physical Society of Japan **76**, 063710 (2007).

49. A. K. Nguyen, R. V. Shchelushkin, and A. Brataas, Physical Review Letters **97**, 136603 (2006).

50. A. K. Nguyen, H. J. Skadsem, and A. Brataas, Physical Review Letters **98**, 146602 (2007).

51. L. Berger, Journal of Applied Physics **55**, 1954 (1984).

52. X. S. Wang, P. Yan, Y. H. Shen, G. E. W. Bauer, and X. R. Wang, Physical Review Letters **109**, 167209 (2012).

53. H. Kohno, G. Tatara, and J. Shibata, Journal of the Physical Society of Japan **75**, 113706 (2006).

54. Y. Tserkovnyak, H. J. Skadsem, A. Brataas, and G. E. W. Bauer, Physical Review B **74**, 144405 (2006).

55. R. A. Duine, A. S. Núñez, J. Sinova, and A. H. MacDonald, Physical Review B **75**, 214420 (2007).

56. X. S. Wang and X. R. Wang, Physical Review B **90**, 184415 (2014).

57. S.-M. Seo, K.-J. Lee, H. Yang, and T. Ono, Physical Review Letters **102**, 147202 (2009).

58. X. P. Wang, C. J. García-Cevera, and E. Weinan, Journal of Computational Physics **171**, 357 (2001).

59. M. J. Donahue and D. G. Porter, *OOMMF User's Guide, Version 1.0*, Interagency Report NISTIR 6376 (National Institute of Standards and Technology, Gaithersburg, MD, USA, 1999) `http://math.nist.gov/oommf/`.

60. A. Vansteenkiste and B. van de Wiele, Journal of Magnetism and Magnetic Materials **323**, 2585 (2011).

61. A. Thiaville, Y. Nakatani, J. Miltat, and Y. Suzuki, Europhysics Letters **69**, 990 (2005).

62. C. Kittel, *Quantum theory of solids* (John Wiley & Sons, 1963).

63. P. Morse and H. Feshbach, *Methods of theoretical physics* (McGraw-Hill, 1953).

64. M. R. Setare and O. Hatami, International Journal of Theoretical Physics **48**, 2164 (2009).

65. R. L. Jaffe, "An algebraic approach to the reflectionless potential in one dimension," (2009), unpublished.

66. J. Lekner, Americal Journal of Physics **75**, 1151 (2007).

67. C. Bayer, H. Schultheiss, B. Hillebrands, and R. L. Stamps, IEEE Transactions on Magnetics **41**, 3094 (2005).

68. Y. Kajiwara, K. Harii, S. Takahashi, J. Ohe, K. Uchida, M. Mizuguchi, H. Umezawa, H. Kawai, K. Ando, K. Takanashi, S. Maekawa, and E. Saitoh, Nature **464**, 262 (2010).

69. H. Hata, T. Taniguchi, H.-W. Lee, T. Moriyama, and T. Ono, Applied Physics Express **7**, 033001 (2014).

70. K.-W. Moon, B.-S. Chun, W. Kim, and C. Hwang, Journal of Applied Physics **114**, 123908 (2013).

71. X.-G. Wang, G.-H. Guo, G.-F. Zhang, Y.-Z. Nie, and Q.-L. Xia, Journal of Applied Physics **113**, 213904 (2013).

72. X.-G. Wang, G.-H. Guo, Y.-Z. Nie, G.-F. Zhang, and Z.-X. Li, Physical Review B **86**, 054445 (2012).

73. J.-S. Kim, M. Stärk, M. Kläui, J. Yoon, C.-Y. You, L. Lopez-Diaz, and E. Martinez, Physical Review B **85**, 174428 (2012).

74. D.-S. Han, S.-K. Kim, J.-Y. Lee, S. J. Hermsdoerfer, H. Schultheiss, B. Leven, and B. Hillebrands, Applied Physics Letters **94**, 112502 (2009).

75. M. Jamali, H. Yang, and K.-J. Lee, Applied Physics Letters **96**, 242501 (2010).

76. D. Wang, X.-G. Wang, and G.-H. Guo, Europhysics Letters **101**, 27007 (2013).

77. X.-G. Wang, G.-H. Guo, G.-F. Zhang, Y.-Z. Nie, and Q.-L. Xia, Applied Physics Letters **102**, 132401 (2013).

78. R. Hertel, W. Wulfhekel, and J. Kirschner, Physical Review Letters **93**, 257202 (2004).

79. A. Thiaville, Y. Nakatani, J. Miltat, and N. Vernier, Journal of Applied Physics **95**, 7049 (2004).

80. O. A. Tretiakov and A. Abanov, Physical Review Letters **105**, 157201 (2010).

81. A. Manchon and S. Zhang, Physical Review B **78**, 212405 (2008).

82. E. Kreyszig, *Advanced engineering mathematics*, 9th ed. (John Wiley & Sons, 2006).

83. W. H. Press, S. A. Teukolsky, W. T. Vetterling, and B. P. Flannery, *Numerical recipes*, 3rd ed. (Cambridge University Press, 2007).

84. MathWorks, MATLAB R2014b Documentation, "Ordinary differential equations," `http://se.mathworks.com/help/matlab/` (2014), [Online; accessed November 22, 2014].

85. MathWorks, MATLAB R2014b Documentation, "Partial differential equations," `http://se.mathworks.com/help/matlab/` (2014), [Online; accessed November 25, 2014].